

# An Analytical Theory of Curriculum Learning in Teacher-Student Networks

Luca Saglietti<sup>†,\*</sup>, Stefano Sarao Mannelli<sup>‡,\*</sup>, and Andrew Saxe<sup>‡,§</sup>

<sup>†</sup> SPOC laboratory, EPFL, Switzerland.

<sup>‡</sup> Department of Experimental Psychology, University of Oxford, Oxford, United Kingdom.

<sup>§</sup> Facebook AI

\* Equal contributions.

## Abstract

In humans and animals, curriculum learning—presenting data in a curated order—is critical to rapid learning and effective pedagogy. Yet in machine learning, curricula are not widely used and empirically often yield only moderate benefits. This stark difference in the importance of curriculum raises a fundamental theoretical question: when and why does curriculum learning help? In this work, we analyse a prototypical neural network model of curriculum learning in the high-dimensional limit, employing statistical physics methods. Curricula could in principle change both the learning speed and asymptotic performance of a model. To study the former, we provide an exact description of the online learning setting, confirming the long-standing experimental observation that curricula can modestly speed up learning. To study the latter, we derive performance in a batch learning setting, in which a network trains to convergence in successive phases of learning on dataset slices of varying difficulty. With standard training losses, curriculum does not provide generalisation benefit, in line with empirical observations. However, we show that by connecting different learning phases through simple Gaussian priors, curriculum can yield a large improvement in test performance. Taken together, our reduced analytical descriptions help reconcile apparently conflicting empirical results and trace regimes where curriculum learning yields the largest gains. More broadly, our results suggest that fully exploiting a curriculum may require explicit changes to the loss function at curriculum boundaries.

## 1 Introduction

Presenting learning materials in a meaningful order according to a curriculum greatly helps learning in humans and animals [1, 2], and is considered an essential aspect of good pedagogy [3]. For example, humans have been shown to learn visual discriminations faster when presented with examples that exaggerate the relevant difference between classes, a phenomenon known as “fading” [4, 5, 6]. Beyond humans, curricula in the form of “shaping” or “staircase” procedures are a near-universal feature of task designs in animal studies, without which training often fails entirely. For instance, the International Brain Laboratory task, a recent standardised perceptual decision-making training paradigm in mice, involves six stages of increasing difficulty before reaching final performance [7].

Building from this intuition, a seminal series of papers proposed a similar curriculum learning approach for machine learning [8, 9, 10]. In striking contrast to the clear benefits of curriculum in biological systems, however, curriculum learning has generally yielded equivocal benefits in artificial systems. Experiments in a variety of domains [11, 12] have found usually modest speed and generalisation improvements from curricula. Recent extensive empirical analyses have found minimal benefits on standard datasets [13]. Indeed, a common intuition in deep learning practice holds that training distributions should ideally be as close as possible to testing distributions, a notion which runs counter to curriculum. Perhaps the only areas where curricula are actively used are in large language models [14] and certain reinforcement learning settings [15].

This gap between the effect of curriculum in biological and artificial learning systems poses a puzzle for theory. When and why is curriculum learning useful? What properties of a task determine the extent of possible benefits? What ordering of learning material is most beneficial? And can new learning algorithms better exploit curricula? Compared to the empirical investigations of curriculum learning, theoretical results on curriculum learning remain sparse. Most notably, [16, 17] show that curriculum can lead to faster learning in a simple setting, but the effects of curriculum on asymptotic generalisation and the dependence on task structure remain unclear. A hint that indeed curriculum learning might lead to statistically different minima comes from a connection between constraint-satisfaction problems and physics results on flow networks [18], but to our knowledge no direct result has been reported in the modern theoretical machine learning literature.

In this work we study the impact of curriculum using the analytically tractable teacher-student framework and the tools of statistical physics [19, 20, 21, 22]. High-dimensional teacher-student models are a popular approach for systematically studying learning behaviour in neural networks [23, 24, 20], and have recently been leveraged to analyse a variety of phenomena [25, 26, 27, 28, 29, 30].

**Contributions.** We analyse a seminal model of curriculum learning first proposed and studied empirically by [10], in which a network learns from high-dimensional data with a sparse subset of task-relevant features amidst a large number of irrelevant factors of variation. We examine the impact of ordering examples by increasing difficulty (curriculum), decreasing difficulty (anti-curriculum), or standard shuffled training, where difficulty is defined as the variance of task-irrelevant features.

- We derive dynamical equations which predict the evolution of test error for online learning under curriculum, anti-curriculum, and standard training. Using these equations, we show that, surprisingly, *both* curriculum and anti-curriculum can speed learning, depending on task parameters and network initialisation.
- We derive test performance in a batch learning setting, where the network trains to convergence on successive dataset slices that vary in difficulty. We show that, while curriculum has no effect for standard training losses, connecting successive learning phases with a Gaussian prior (or equivalently,  $L_2$  penalty) between weights can result in a large improvement in test performance. Again, we find that *both* curriculum and anti-curriculum can improve test performance, though curriculum helps more.
- Building from these basic analyses, we trace the impact of curriculum in several broader settings, including tasks with different fractions of task-relevant features, curricula with more than two stages, and experiments with real world datasets (based on CIFAR10).

## 2 Model definition and overview of approach

In the following, we revisit a prototypical model of curriculum learning from [10]. Our setting is summarised in Fig. 1. The model entails a simple teacher-student setup, where teacher and student are each shallow 1-layer neural networks of size  $N$  (also known as perceptrons). The learning task for the student is a binary classification problem, with dataset  $\mathcal{D} = \{(y^\mu, \mathbf{x}^\mu)\}_{\mu=1}^M$ , where the ground-truth labels are produced by the teacher network  $y^\mu = \text{sign } \mathbf{W}_T \cdot \mathbf{x}^\mu$ . A key feature of this model is that the teacher network is sparse, with only a fraction  $\rho < 1$  of  $\sim \mathcal{N}(0, 1)$  non-zero components. Therefore, in order to achieve a good test accuracy, the student has to guess which components should be set to zero and align the relevant weights in the correct direction. Any sparsity  $0 < \rho < 1$  could in principle give rise to the phenomenology we seek to analyse. In the remainder of the paper we will focus on the case  $\rho = 0.5$ .

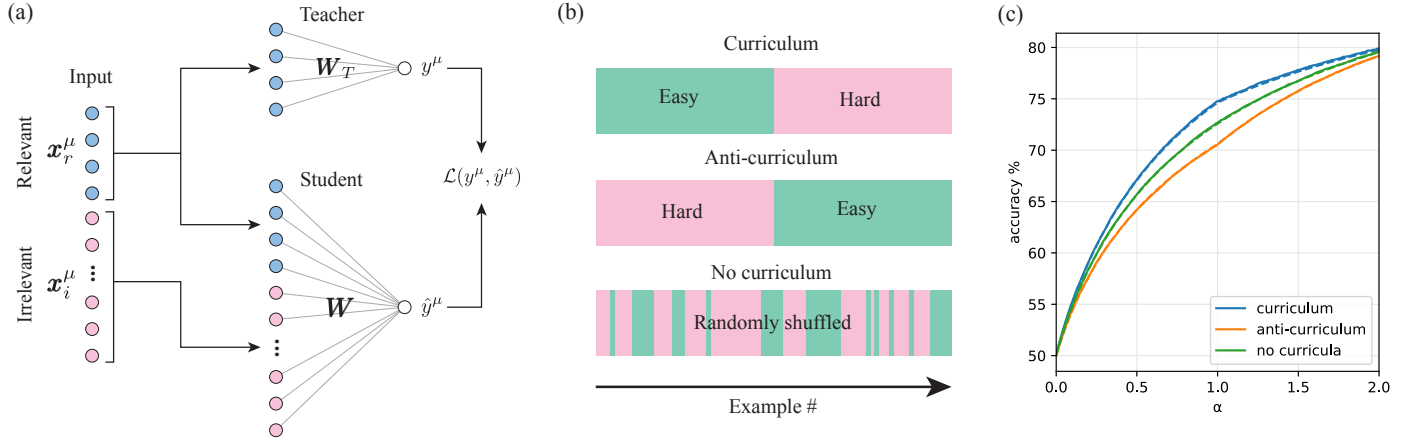


Figure 1: **Teacher-student setting for curriculum learning.** (a) Illustration of teacher-student setting in which a “student” network is trained from *i.i.d.* inputs with labels from a “teacher” network. Since the teacher network is sparse, its output depends only on a subset of *relevant* input features. (b) We consider curricula which order examples by difficulty, here taken to be the variance in the irrelevant feature dimensions. We refer to increasing, decreasing, and random difficulty order as curriculum, anti-curriculum, and no curriculum, respectively. (c) Example test error on hard examples for the student over training. Solid lines show numerical simulations, while dashed lines show theoretical predictions derived in Section 3. For this particular parameter setting, curriculum speeds learning but only modestly improves final performance at  $\alpha = 1$ . Parameters:  $\alpha_1 = 1$ ,  $\alpha_2 = 1$ ,  $\Delta_1 = 0$ ,  $\Delta_2 = 1$ ,  $\gamma = 10^{-5}$ ,  $\eta = 3$ .

We model the variable degree of difficulty in the samples by decomposing each input vector as  $\mathbf{x}^\mu = [\mathbf{x}_r^\mu, \mathbf{x}_i^\mu] \in \mathbb{R}^N$ , where  $\mathbf{x}_r^\mu \in \mathbb{R}^{\rho N}$  denotes the relevant components of the input, and  $\mathbf{x}_i^\mu \in \mathbb{R}^{(1-\rho)N}$  the irrelevant ones. Note that, crucially, the sparse teacher network is completely blind to the irrelevant part of the input:  $y^\mu = \text{sign} \sum_{j=1}^{\rho N} W_{T,j} x_{r,j}^\mu$ . While  $x_{r,j}^\mu \sim \mathcal{N}(0, 1)$ ,  $\forall \mu$ <sup>1</sup>, we consider the variance for the irrelevant components to be sample-dependent  $x_{i,j}^\mu \sim \mathcal{N}(0, \Delta^\mu)$ . Note that a smaller variance in the irrelevant part induces a higher SNR in the student learning problem.

The dataset is partitioned according to difficulty levels given by the variances of the irrelevant inputs. For simplicity we consider only two partitions in most of our analysis, but generalisations to more difficulty levels follow straightforwardly. We have a dataset with  $M = (\alpha_1 + \alpha_2)N$  total samples, in which the irrelevant inputs of the first  $\alpha_1 N$  samples have variance  $\Delta_1$ , and the remaining  $\alpha_2 N$  samples have variance  $\Delta_2 > \Delta_1$ . In the curriculum learning condition we present the easy examples first, while in the anti-curriculum condition we present the hard examples first. Standard learning presents examples shuffled in random order.

### 3 Online dynamical solution in the large input limit

We start by focusing on the same online learning setting explored in [10]. We consider a 1-layer student network with sigmoidal activation function,  $\sigma(\cdot) = \text{erf}(\cdot/\sqrt{2})$ , that learns to minimise a mean square error loss with  $L_2$  regularisation of intensity  $\gamma$ , using gradient descent. This yields the weight update

$$\mathbf{W}^{\mu+1} = \mathbf{W}^\mu - \frac{\eta}{\sqrt{N}} \sigma' \left( \frac{\mathbf{W} \cdot \mathbf{x}^\mu}{\sqrt{N}} \right) \left( \sigma \left( \frac{\mathbf{W} \cdot \mathbf{x}^\mu}{\sqrt{N}} \right) - y^\mu \right) \mathbf{x}^\mu - \gamma \mathbf{W}^\mu. \quad (1)$$

The dynamics of the model can be analysed in the high-dimensional limit  $N \rightarrow \infty$ . Generalising the results of [24, 31] on the online stochastic gradient descent dynamics in single-layer regression problems, we obtain a precise description of the performance at all times, as a function of several order parameters: the squared norm

<sup>1</sup>In [10] the distribution of relevant and irrelevant inputs is uniform between 0 and 1, but this difference does not qualitatively change the results.

of the relevant and irrelevant part of the student weights  $Q_r = \frac{1}{N} \mathbf{W}^r \cdot \mathbf{W}^r$  and  $Q_i = \frac{1}{N} \mathbf{W}^i \cdot \mathbf{W}^i$ , respectively; the overlap of the relevant weights of the student and teacher  $R = \frac{1}{N} \mathbf{W}^r \cdot \mathbf{W}_T$ ; and the squared norm of the teacher vector  $T = \frac{1}{N} \mathbf{W}_T \cdot \mathbf{W}_T$ . In particular, given  $Q_r$ ,  $Q_i$ ,  $R$  and  $T$ , the test loss (i.e. average loss on a new example) on a dataset with variance  $\Delta$  in the irrelevant inputs is given by

$$\mathcal{L}_{\text{MSE}} = \frac{1}{2} + \frac{1}{\pi} \sin^{-1} \left( \frac{Q_r + \Delta Q_i}{1 + Q_r + \Delta Q_i} \right) - \frac{2}{\pi} \sin^{-1} \left( \frac{R}{\sqrt{T(Q_r + \Delta Q_i + 1)}} \right), \quad (2)$$

the accuracy by

$$\mathcal{A} = \mathbb{E} \left[ \frac{1}{2} (y \text{ sign } \hat{y} + 1) \right] = \frac{1}{2} + \frac{1}{\pi} \sin^{-1} \left( \frac{R}{\sqrt{T(Q_r + \Delta Q_i)}} \right), \quad (3)$$

and the overlap between teacher and student by  $m = R/\sqrt{T(Q_r + Q_i)}$ . If the dataset contains a random mixture of different difficulty levels  $\Delta_1, \Delta_2, \dots$ , the loss and accuracy can be obtained by taking a weighted average over the partitions.

To understand how test performance changes through learning, we focus on the evolution of the order parameters. Combining their definition with the definition of the online dynamics Eq. (1) and the fact that the random variables concentrate in the high-dimensional limit ( $N \rightarrow \infty$ ), we obtain an analytic form for the updates:

$$Q_r[k+1] = f_{Q_r}(Q_r[k], Q_i[k], R[k], T), \quad (4)$$

$$Q_i[k+1] = f_{Q_i}(Q_r[k], Q_i[k], R[k], T), \quad (5)$$

$$R[k+1] = f_R(Q_r[k], Q_i[k], R[k], T), \quad (6)$$

where  $f_{Q_r}$ ,  $f_{Q_i}$  and  $f_R$  are long but straightforward analytical expressions that are reported in the supplementary material (SM).

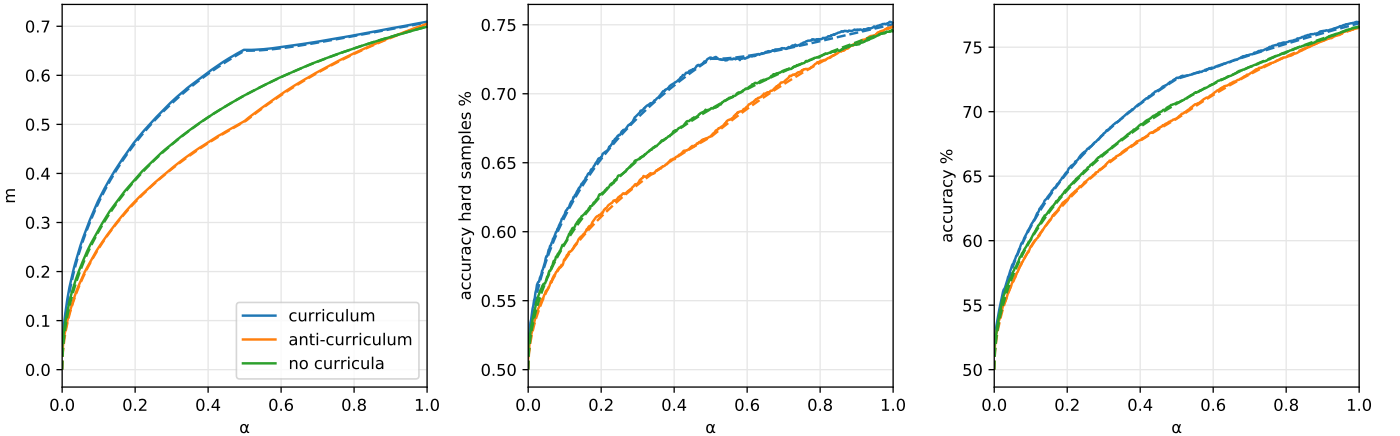
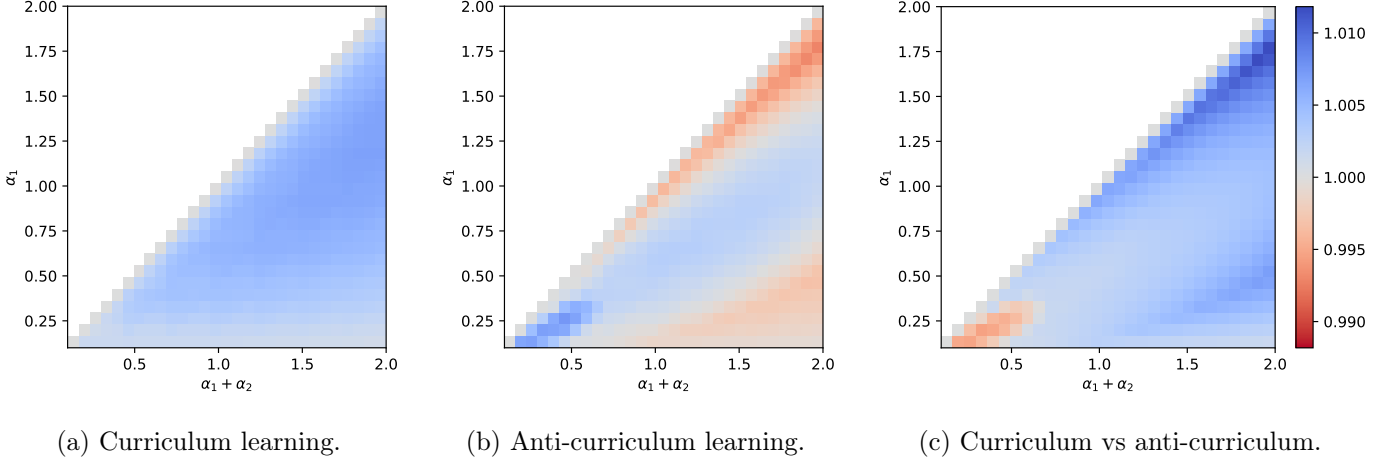


Figure 2: **Online learning trajectories under different curricula.** Average dynamics under curriculum (blue), anti-curriculum (orange), and no curriculum (green), with parameters  $\rho = 0.5$ ,  $\alpha_1 = 0.5$ ,  $\Delta_1 = 0.0$ ,  $\alpha_2 = 0.5$ ,  $\Delta_2 = 1.0$ . The figures show the overlap with the teacher (left), the accuracy on hard samples (mid) and overall accuracy (right). The solid lines are the average of 500 simulations with input dimension  $N = 500$  and the dashed lines come from the theoretical result, Eqs. (3)-(6). The learning rate, variance at initialisation and weight decay are set to the optimal value.

**Dynamical advantages of curriculum.** With these theoretical results in hand, we now characterise the performance of curricula in the online setting. The dynamical equations have two key advantages relative to

simulating models in this setting. First, they are free of finite size effects and stochastic fluctuations. And second, their evaluation is very fast, enabling systematic exploration of the parameter space of the problem, along with fine-grained optimisation over hyper-parameters such as learning rate, weight decay and scaling in the initialisation.



**Figure 3: Phase diagram of online learning performance gap with optimal parameters.** The colour scale shows the ratio of the accuracy on hard instances reached by curriculum over no-curriculum (left), anti-curriculum over no-curriculum (center), and curriculum over anti-curriculum (right), as a function of the total dataset size ( $\alpha_1 + \alpha_2$ ) and easy dataset size ( $\alpha_1$ ). Curriculum broadly benefits performance and anti-curriculum is effective in certain regions, but the size of the improvement is modest. Parameters:  $\rho = 0.50$ ,  $\Delta_1 = 0$ ,  $\Delta_2 = 1$ .

Optimising final test accuracy separately for each curriculum strategy, we find that curriculum learning is the optimal strategy, followed by baseline (no-curriculum) and lastly anti-curriculum. In Fig. 2 we show typical learning trajectories for a dataset with equal numbers of easy and hard samples. The results of the simulations (solid lines) are well-described by our theoretical equations (dashed lines), and show that the curriculum strategy leads to better performance throughout training. Fig. 2a shows the cosine angle  $m$  between teacher and student weights. In our setting,  $m$  directly measures the student network’s alignment with the ground-truth rule given by the teacher. This quantity is more complicated for more complex architectures and not available in real settings. A good proxy for  $m$  is the accuracy measured only on hard instances in the dataset, given in Fig. 2b, which can be used in practical cases. The accuracy evaluated on the whole dataset, given in Fig. 2c, is a less sensitive measure of alignment because easy instances can be correctly classified even with suboptimal weights. In the remainder, therefore, we focus on accuracy evaluated on hard examples.

Next we systematically trace the effect of curriculum for a range of total dataset sizes ( $\alpha_1 + \alpha_2$ ) and number of easy examples  $\alpha_1$  in the phase diagram in Fig. 3. This diagram shows on the left (center) the accuracy on hard instances reached at the end of training by curriculum learning (anti-curriculum learning respectively) normalised by the accuracy reached by the standard strategy. The two heatmaps show that curriculum learning always outperforms standard learning and that, on the other hand, anti-curriculum learning outperforms standard learning only in part of the diagram. The right panel of Fig. 3 shows that only a small part of the phase diagram is dominated by anti-curriculum learning, while in the majority of situations curriculum learning is the best strategy. Interestingly, there is a sizeable region of the diagram in which *both* curriculum and anti-curriculum help, possibly explaining why both have been recommended in prior work [10, 12, 32, 33, 34].

Further, we find that our setting, in which a small task-relevant signal is embedded in large task-irrelevant variation, is critical to the benefit of curriculum. Fig. C.1 of the SM shows performance as a function of sparsity  $\rho$ . Non-sparse tasks do not benefit. Hence curriculum aids tasks with many irrelevant factors of variation. Interestingly, the literature from human psychology shows precisely this: no curriculum benefits for low-D tasks or tasks with no variation in irrelevant dimensions [4].

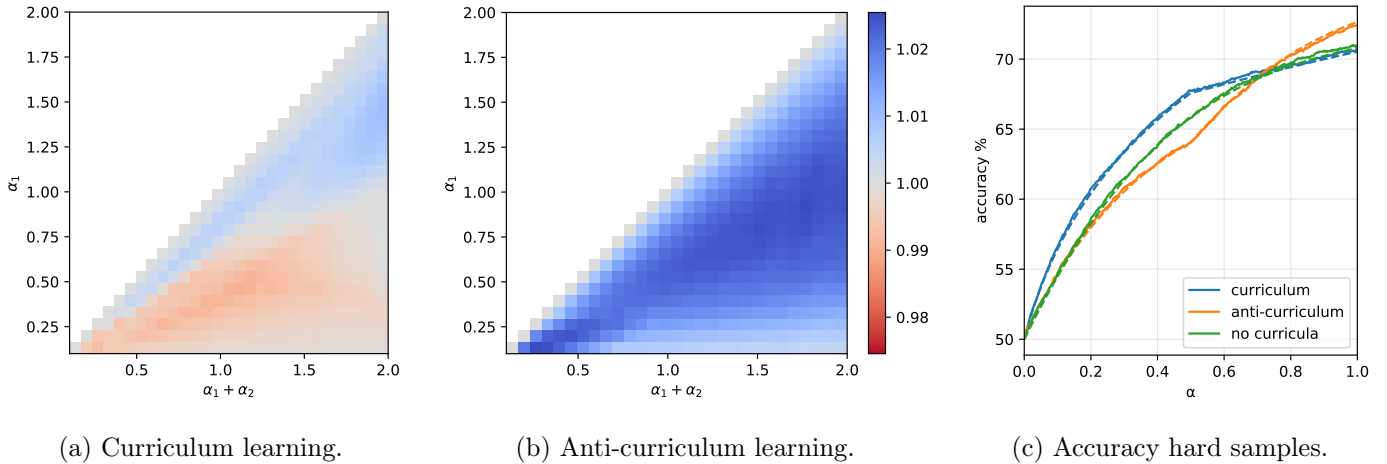


Figure 4: **Performance gap starting from high initialisation.** The first two figures show the accuracy-gap on hard instances between curriculum learning and the baseline (left) and anti-curriculum learning and the baseline (center). The right panel shows the accuracy for  $\alpha_1 = \alpha_2 = 0.5$ .

Our results also highlight the intricate dependence of curriculum on parameters of the learning setup. If not all parameters are correctly optimised, we can observe more complex scenarios. For instance, anti-curriculum learning is always the best strategy starting from a large initialisation, as Fig. 4 shows for weights of order 1. In this case, curriculum learning shows an advantage only in the first phase when easy examples are shown (right panel), which is consistent with the results of [17]. However, in the next phase when hard examples are shown, the curriculum strategy does not extract enough information and it is outperformed by the other two strategies. The fact that curriculum or anti-curriculum can look better depending on other learning parameters like initialisation might help explain the confusion in the literature over the best protocol [10, 12, 32, 33, 34]. At least in this model, better performance from anti-curriculum is a signature of a sub-optimal choice of the parameters. To summarise our findings in this online learning setting, curriculum mainly offers a *dynamical advantage*: it speeds learning, with only minimal impact on asymptotic performance.

## 4 Batch learning solution

The previous section discussed the online case where each example is used once and then discarded. However, in common practice in machine learning, neural networks typically revisit each sample repeatedly until convergence. Therefore an important question is: *can curricula lead to a generalisation improvement when trained on the same dataset until convergence?*

We investigate this question by considering a student model that learns from slices of a dataset in distinct optimisation phases, where in each phase the student optimises a  $L_2$ -regularised logistic loss. Without further modification, curriculum can have no effect in this setting: due to the convex nature of the teacher-student setup [20], the network is bound to converge to a minimum uniquely determined by the final slice of data, with no memory of the progress made at intermediate steps. This simple observation may help explain empirical observations on real data, such as [13], which find no benefit of curriculum in standard settings (though we note that curriculum could still influence non-convex problems [10]). This observation raises the theoretical question of how curriculum learning could induce a non-vanishing effect in batch learning settings.

To instantiate a memory effect in our model, we propose biasing the optimisation landscape via a Gaussian prior, centred around the optimiser of the previous learning phase. The additional term in the loss acts as an elastic coupling between the successive phases, and the associated intensity  $\gamma_{12}$  is then an additional hyper-parameter of the model. This scheme is similar to regularisation methods proposed against catastrophic interference in continual learning, such as Synaptic Intelligence [35].



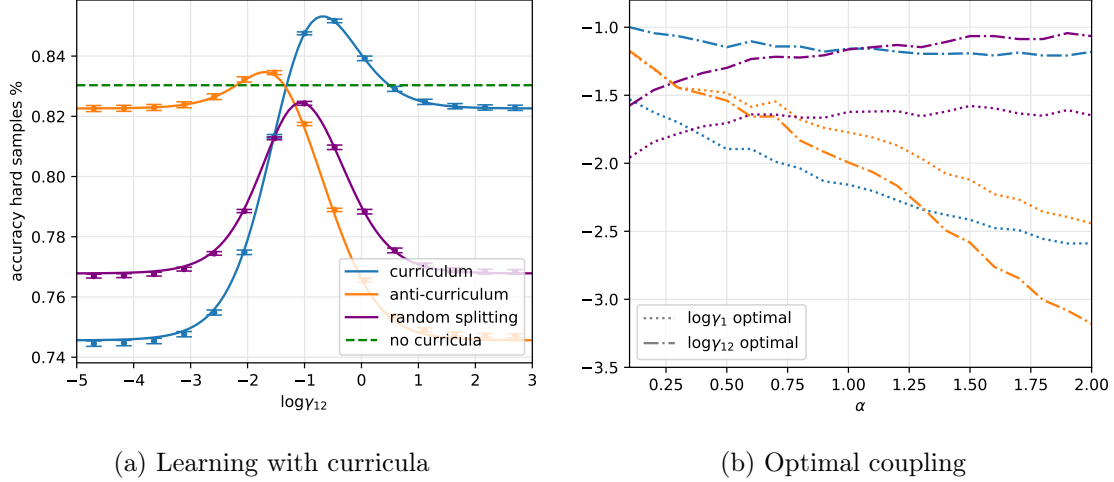


Figure 5: **Effect of elastic coupling (Gaussian prior) between curriculum phases.** (Left) comparison between asymptotic performance of curricula (full lines) and single batch learning, at  $\alpha_1 = 1$   $\alpha_2 = 1$ , with a regularisation  $\gamma_1$  that yields the best generalisation when learning the entire dataset (in principle not optimal for the other strategies). The points represent the results from 10 numerical simulations at size  $N = 2000$ . (Right) Optimal values for  $\gamma_{12}$  (dash-dotted lines) and  $\gamma_1 = \gamma_2$  (dotted lines) for balanced datasets ( $\alpha_1 = \alpha_2$ ) of increasing size. Parameters:  $\rho = 0.50$ ,  $\Delta_1 = 0$  and  $\Delta_2 = 1$ .

Tools from statistical physics can be used to analytically compute test performance under this scheme. In order to simplify the presentation, we first consider just two learning phases. It is natural to frame this setting as a 2-level problem, involving two systems with independent copies of the network weights  $\mathbf{W}_1$  and  $\mathbf{W}_2$ . In a typical statistical physics approach, we associate a Boltzmann-Gibbs measure to the systems, with an energy function determined by the regularized logistic loss  $\mathcal{L}_\gamma$ . While the statistical properties of the first system can be determined self-consistently, the added elastic interaction creates a dependence of the second measure on the configurations of the first system. In mathematical terms, the coupled system is represented by the following partition function:

$$\langle Z(\mathbf{W}_2, \mathbf{W}_1; \mathcal{D}_1, \mathcal{D}_2) \rangle_{\mathbf{W}_1} = \int d\mathbf{W}_1 \frac{e^{-\beta_1 \mathcal{L}_{\gamma_1}(\mathbf{W}_1, \mathcal{D}_1)}}{Z_1(\mathbf{W}_1)} \log \int d\mathbf{W}_2 e^{-\beta_2 (\mathcal{L}_{\gamma_2}(\mathbf{W}_2, \mathcal{D}_2) + \frac{\gamma_{12}}{2} \|\mathbf{W}_2 - \mathbf{W}_1\|_2^2)}, \quad (7)$$

where  $\mathcal{D}_1, \mathcal{D}_2$  denote the two dataset slices. This object represents the normalisation of the Boltzmann-Gibbs measure, and allows one to extract relevant information on the asymptotic behaviour of our model. The optimisations entailed in each learning phase can be described in the “low noise” limit of  $\beta_1, \beta_2 \rightarrow \infty$ , where the measures focus on the minimizers of the respective losses. In order to study a self-averaging quantity that does not depend on a specific realisation of the dataset, we aim to compute the associated average free-energy:

$$\Phi = \lim_{N \rightarrow \infty} \lim_{\beta_1, \beta_2 \rightarrow \infty} \frac{1}{\beta_2 N} \langle \log \langle Z(\mathbf{W}_2, \mathbf{W}_1; \mathcal{D}_1, \mathcal{D}_2) \rangle_{\mathbf{W}_1} \rangle_{\mathcal{D}_1, \mathcal{D}_2}. \quad (8)$$

This quantity can be seen as a special case of the so-called Franz-Parisi potential computation [36, 37], and the entailed double average can be evaluated through the replica method. Refer to SM for details.

Similar to the online case, in high-dimensions the free-entropy concentrates on a deterministic function that depends on several order parameters that capture the geometrical distribution of teacher and student configurations. In addition to those already introduced above, we also have  $\delta Q$ , which is linked to the variance of the student norm. Moreover, for each order parameter we also need to introduce a conjugate parameter, denoted in the following with the hat symbol. The final expression for the free-energy reads:

$$\Phi = \text{extr} \left[ - \left( \hat{R} R + \frac{1}{2} \left( \left( \hat{Q} \delta Q - \delta \hat{Q} Q \right)_{r+i} \right) \right) + g_S(\gamma_1, \gamma_2, \gamma_{12}) + \alpha_1 g_E(\Delta_1) + \alpha_2 g_E(\Delta_2) \right] \quad (9)$$

where  $g_S$  and  $g_E$  are two scalar functions, often called entropic and energetic channels, that encode the dependence of the optimisation problem on the Gaussian prior and the logistic loss respectively.

The extremum condition for the free-energy yields a system of fixed-point equations that converge to an asymptotic prediction for the order parameters, comparable with the results of numerical simulations on large instances. At convergence, the order parameters can be inserted again in Eq. 3 to obtain an estimate of the test accuracy. Note that this formalism is not limited to two phases, but can be extended to the case of a discrete number of sequential stages, each one coupled only to the previous one.

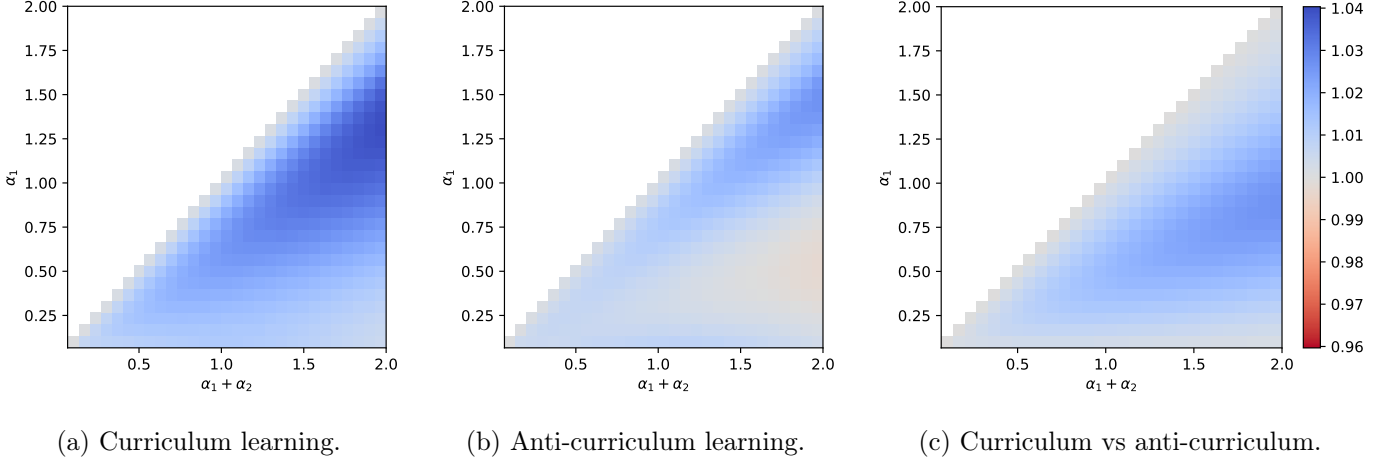


**Figure 6: Phase diagram for the performance gap in the batch setting.** The colour scale shows the ratio of the accuracy on hard instances for curriculum over no-curriculum (left), anti-curriculum over no-curriculum (center), and curriculum over anti-curriculum (right), as a function of the total dataset size ( $\alpha_1 + \alpha_2$ ) and easy dataset size ( $\alpha_1$ ). In contrast to the online case, performance benefits are greater and curriculum is strictly better than anti-curriculum. Both  $\gamma_1 = \gamma_2$  and  $\gamma_{12}$  are optimised point-wise, in order to yield the best test accuracy. Parameters:  $\rho = 0.50, \Delta_1 = 0, \Delta_2 = 1$ .

**Asymptotic advantages of curriculum.** In Fig. 5 we investigate the effect of the coupling strength for a dataset composed of easy and hard examples in equal proportions. The left panel shows a comparison of curriculum and anti-curriculum performance with the base-line performance, i.e. when all the examples are learned in a single batch. The  $L_2$  regularisation is set in all stages equal to the value  $\gamma_{1,opt}$  that maximises accuracy in the single batch scenario. We clearly observe a range of values of  $\gamma_{12}$  where curricula become beneficial and, contrary to the small effect seen in the dynamical section ( $\sim 1\%$  accuracy gain), the prior induces up to 4% improvement. Note that even anti-curriculum strategies are found to outperform the single-batch baseline. Since the prior adds an extra parameter in the model, one may wonder whether the improvement comes from the additional degree of freedom. We exclude this possibility by considering a 2-phase setting where the dataset is sliced randomly. The corresponding line falls below the baseline, confirming that the key to the improvement is indeed the grouping of examples by difficulty. In Fig. 5b, we show the optimal values of  $\gamma_{12}$  for the different curricula, with balanced datasets of increasing size. The results confirm the intuition that a positive coupling should always prove beneficial, since it is the only way of preserving the information gained in the former learning stage.

Contrary to the online SGD case, batch learning with elastic coupling notably improves test accuracy of both curriculum and anti-curriculum above the baseline. Fig. 6 shows similar phase diagrams to Fig. 3 but for the batch setting. At each point in the phase diagram the regularisation level  $\gamma_1 = \gamma_2$  and the coupling  $\gamma_{12}$  are optimised to yield the best accuracy. In batch learning the performance order appears to be nearly always preserved: curriculum followed by anti-curriculum followed by baseline.

A natural generalisation of this reasoning, to 3 or more difficulties in the dataset, would suggest that it is best to present data in order of difficulty. We investigated this question again for 3 splits and surprisingly found



that the situation is more complicated, as the results depend on the relative sizes of the partitions. In Fig. 7 we observe that the best ordering can change: the three images represent three different partition sizes and e.g. what is the best strategy in the figure on the left appears to be among the worst in the figure on the right. Qualitatively, as the ratio between the slices (from easy to hard) gets smaller, the curriculum ordering becomes more convenient. Instead, when the ratio is large it might be better to throw away the more complex data and just focus on the simpler part of the dataset.

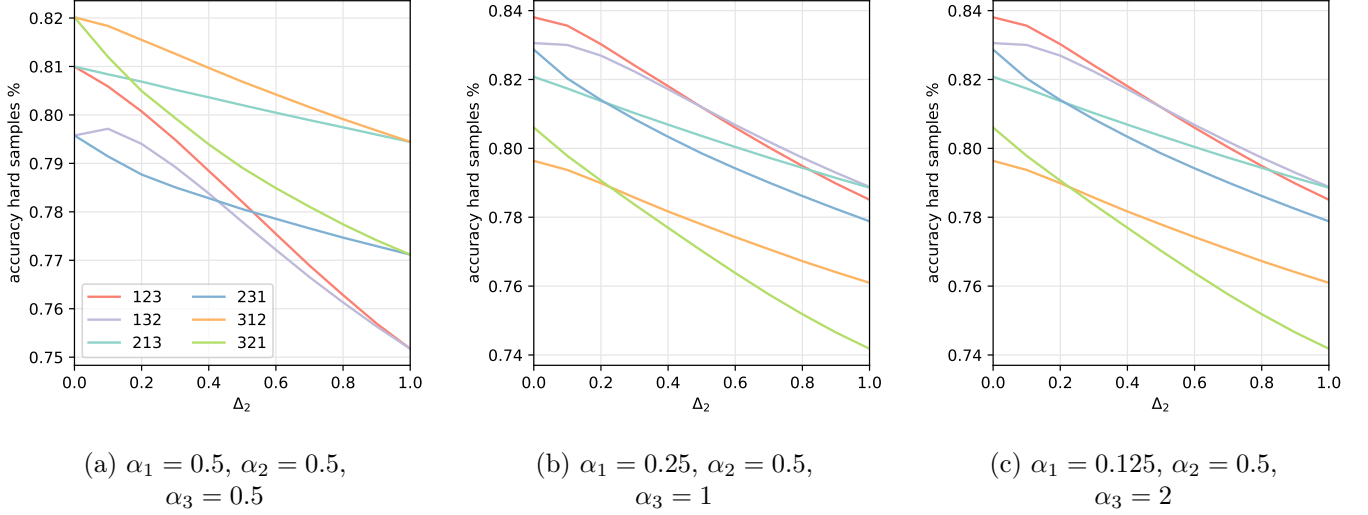


Figure 7: **Learning in multiple stages.** In these experiments we set  $\rho = 0.5$ ,  $\Delta_1 = 0$ ,  $\Delta_3 = 1$  and  $\Delta_2$  is varied. The three figures show different ratios  $R$  between the dataset slices: (left)  $R = 1$ , (mid)  $R = 0.5$ , (right)  $R = 0.25$ . The hyperparameters  $\gamma_1, \gamma_2, \gamma_3, \gamma_{12}, \gamma_{23}$  are set to (locally) optimal values.

## 5 Rethinking curriculum learning with elastic coupling

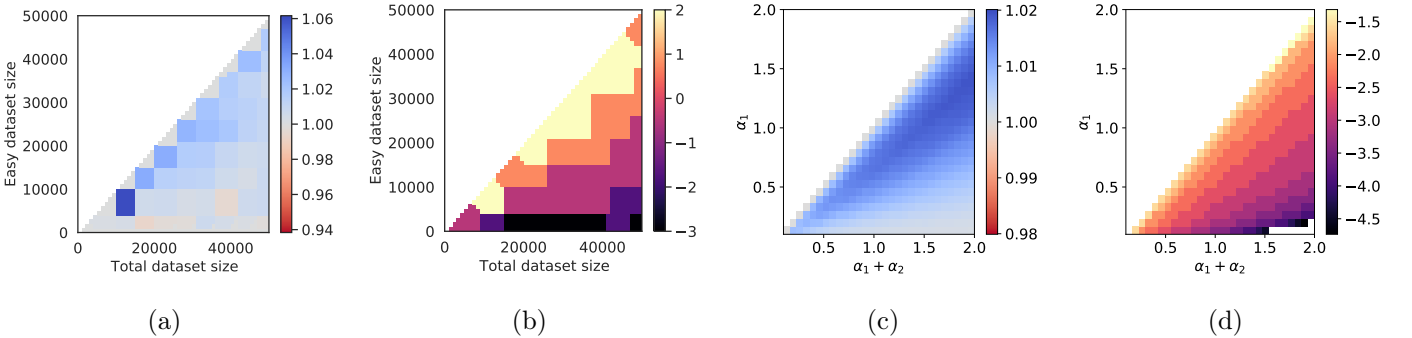


Figure 8: **Phase diagrams with elastic coupling on real data & for online learning.** Panels (a,b) show CIFAR10-derived task, panels (c,d) show online learning. Panels (a,c) show the ratio between final accuracy on hard instances reached using curriculum learning and the standard strategy, panels (b,d) show the optimal coupling  $\gamma_{12}$  in log-scale.  $\eta, \gamma, \gamma_{12}$ , init, and stopping time are optimised.

**Real data.** Finally we apply curriculum learning with priors on real data. We construct a test case derived from the CIFAR10 dataset [38] by patching two images together into a  $32 \times 64$  input image. The network has to learn that the classification depends only on the left image, while the right image is a distractor that is irrelevant to the classification. The easy and hard instances are obtained by reducing the brightness of the distractor (see SM for example inputs). The architecture is a single-layer network trained with the cross-entropy loss and

the curriculum protocol with Gaussian prior between the two stages. Weights are optimised using SGD and momentum, with an annealed learning rate. All training parameters are optimised, and full details are presented in the SM.

Fig. 8 (a,b) shows the ratio between the final validation accuracy on hard samples reached by curriculum and standard learning. The curriculum strategy leads to an improvement of up to 6% that gradually decreases with the dataset size. As in the results on the synthetic model, the maximal advantage is achieved close to the diagonal, where the dataset contains a large number of easy examples, and decreases away from the diagonal (as the number of hard instances increases). Fig. 8b shows the logarithm of the optimal coupling  $\gamma_{12}$ . The coupling is stronger close to the diagonal and weaker away. This is reasonable since when more easy examples are available, the solution found after the first phase is higher quality, justifying a strong bias toward the weights obtained at the end of the first phase. This setting may also help explain the minimal benefits of curriculum in standard datasets [13]: most vision datasets arguably contain an implicit curriculum in which objects are already cropped to remove clutter. Consistent with this, in human development, infants must initially slowly learn object names in extensive clutter [39, 40] and exhibit a burst in vocabulary when they can grasp and centre objects in view [41, 42].

**Online learning.** Motivated by the results on batch-learning, we reconsider the online setting and add elastic coupling between the two phases of learning. This leads to a modification of the dynamical equations and introduces two additional order parameters  $S_r = \frac{1}{N} \mathbf{W}_1^r \cdot \mathbf{W}_2^r$  and  $S_i = \frac{1}{N} \mathbf{W}_1^i \cdot \mathbf{W}_2^i$  that measure the overlap between the weights in the first and second stage of the dynamics. In the high-dimensional limit we can obtain the exact dynamics and all the details are reported in the SM. Figs. 8 (c,d) shows that the coupling leads to a stronger improvement of the final accuracy (third panel). Contrary to the findings in Fig. 3, curriculum is always the optimal strategy to use and the final accuracy has increased by an additional 1%. In the last panel we observe the logarithm of the optimal coupling. Both panel c and d of Fig. 8 are similar to their counterparts on real data given by panels (a,b), and the same observations apply.

## Final considerations & broader impacts

By deriving new analytical results on the performance of learning under different curricula in a simple setting, we showed that the use of priors connecting curriculum phases leads to strong improvement in the three settings considered: online learning, batch learning, and a simple real data setting. Our work is theoretical in nature and these results are limited to very simple architectures. Nevertheless, they suggest rethinking the loss function to better exploit curriculum strategies. Taking into account the heterogeneity of the samples in the loss may lead to improvements also in more complex architectures and on real data. We hope this work will inspire future algorithms that can better exploit curricula.

The present study is primarily theoretical, and we do not foresee any direct negative social impact resulting from this research. More broadly, beyond improving machine learning methods, better understanding of the impact of curricula on learning could help aid curriculum design in educational contexts. Conversely, it could aid design of adversarial curricula meant to disrupt or bias learning. At present, our work is far from these impacts.

## Acknowledgement

We thank Miguel Ruiz-Garcia and Ronald Dekker for precious discussions. We acknowledge funding from the ERC under the European Union’s Horizon 2020 Research and Innovation Program Grant Agreement 714608-SMiLe, and a Sir Henry Dale Fellowship from the Wellcome Trust and Royal Society (grant number 216386/Z/19/Z). A.S. is a CIFAR Azrieli Global Scholar in the Learning in Machines & Brains programme.

# Supplemental Material

## A State evolution of the online dynamics

In this section we show how to derive the dynamical equations for the online dynamics. The equations given in an implicit form in the main text,  $f_{Q_r}, f_{Q_i}, f_R$ , are reported explicitly at the end of the next section, Eqs. (A.23-A.25). Finally, in the subsequent section, we comment on how the state evolution is modified to deal with the Gaussian priors and we derive the new dynamical equations for that case.

**Derivation** We follow the derivation proposed in [24, 31] to derive the averaged high-dimensional dynamical equations. The student is a 1-layer network that minimises sample-wise the square error

$$\mathcal{L}^\mu = \frac{1}{2} (y^\mu - \hat{y}^\mu)^2 \doteq \frac{1}{2} (\delta^\mu)^2. \quad (\text{A.1})$$

Given  $\phi(\cdot) = \text{sign}(\cdot), \sigma(\cdot) = \text{erf}(\cdot/\sqrt{2})$ , the online stochastic gradient descent updates are

$$\mathbf{W}^{\mu+1} = \mathbf{W}^\mu - \frac{\eta}{\sqrt{N}} \sigma'(\lambda_r^\mu + \lambda_i^\mu) \delta^\mu \mathbf{x}^\mu, \quad (\text{A.2})$$

with

$$\lambda_r^\mu = \frac{1}{\sqrt{N}} \mathbf{W}_r \cdot \mathbf{x}_r^\mu, \quad (\text{A.3})$$

$$\lambda_i^\mu = \frac{1}{\sqrt{N}} \mathbf{W}_i \cdot \mathbf{x}_i^\mu, \quad (\text{A.4})$$

$$\rho^\mu = \frac{1}{\sqrt{N}} \mathbf{W}_T \cdot \mathbf{x}_r^\mu. \quad (\text{A.5})$$

The evolution of the dynamics can be tracked using 4 order parameters:

$$Q_r = \frac{1}{N} \mathbf{W}_r \cdot \mathbf{W}_r, \quad (\text{A.6})$$

$$Q_i = \frac{1}{N} \mathbf{W}_i \cdot \mathbf{W}_i, \quad (\text{A.7})$$

$$R = \frac{1}{N} \mathbf{W}_r \cdot \mathbf{W}_T, \quad (\text{A.8})$$

$$T = \frac{1}{N} \mathbf{W}_T \cdot \mathbf{W}_T; \quad (\text{A.9})$$

representing the overlaps between the weights of student (relevant and irrelevant parts) and teacher.

The evolution of those follow from the definition of the dynamics Eq. (A.2). In the high-dimensional limit the random variables in the problem concentrates around the mean, therefor to the leading order we have the following equations

$$Q_r[k+1] = Q_r[k] + \frac{1}{N} [2\eta \mathbb{E}[\delta \sigma'(\lambda_r + \lambda_i) \lambda_r] + \rho \Delta \eta^2 \mathbb{E}[\delta^2 \sigma'(\lambda_r + \lambda_i)^2]]; \quad (\text{A.10})$$

$$Q_i[k+1] = Q_i[k] + \frac{1}{N} [2\eta \mathbb{E}[\delta \sigma'(\lambda_r + \lambda_i) \lambda_i] + (1 - \rho) \Delta \eta^2 \mathbb{E}[\delta^2 \sigma'(\lambda_r + \lambda_i)^2]]; \quad (\text{A.11})$$

$$T[k+1] = T[k] + \frac{1}{N} [\eta \mathbb{E}[\delta \sigma'(\lambda_r + \lambda_i) \rho]]. \quad (\text{A.12})$$

(A.13)

Where the expectation acts with respect to all the stochastic variables. In order to obtain explicit formulae we need to evaluate those averages. The random variables in the equations –  $\lambda_r$ ,  $\lambda_i$  and  $\rho$  – are Gaussian with zero mean, to characterise them we only need their covariance:

$$\Sigma_{\lambda_r, \lambda_i, \rho} = \begin{pmatrix} Q_r & 0 & R \\ 0 & Q_i & 0 \\ R & 0 & T \end{pmatrix}.$$

In order to derive analytical expression we must evaluate the expected values:  $\mathbb{E}[\phi(\rho)\sigma'(\lambda)\rho]$ ,  $\mathbb{E}[\phi(\rho)\sigma'(\lambda)\lambda]$ ,  $\mathbb{E}[\sigma(\lambda)\sigma'(\lambda)\rho]$ ,  $\mathbb{E}[\sigma(\lambda)\sigma'(\lambda)\lambda]$ ,  $\mathbb{E}[\phi(\rho)^2\sigma'(\lambda)^2]$ ,  $\mathbb{E}[\sigma(\lambda)^2\sigma'(\lambda)^2]$ , and  $\mathbb{E}[\phi(\rho)\sigma(\lambda)\sigma'(\lambda)^2]$ . Where  $\sigma$  is the activation function of the student and  $\phi$  is the activation function of the teacher (in particular  $\phi(\cdot) = \text{sign}(\cdot)$  for classification).

$$\mathbb{E}[\phi(\rho)\sigma'(\lambda)\rho] = \frac{2}{\pi} \frac{\sqrt{T(Q_r + Q_i + 1) - R^2}}{Q_r + Q_i + 1} \quad (\text{A.14})$$

$$\mathbb{E}[\phi(\rho)\sigma'(\lambda)\lambda_r] = \frac{2}{\pi} \frac{R(Q_i + 1)}{Q_r + Q_i + 1} \frac{1}{\sqrt{T(Q_r + Q_i + 1) + R^2}}. \quad (\text{A.15})$$

$$\mathbb{E}[\phi(\rho)\sigma'(\lambda)\lambda_i] = -\frac{2}{\pi} \frac{RQ_i}{Q_r + Q_i + 1} \frac{1}{\sqrt{T(Q_r + Q_i + 1) + R^2}}. \quad (\text{A.16})$$

$$\mathbb{E}[\sigma(\lambda)\sigma'(\lambda)\rho] = \frac{2}{\pi} \frac{R}{Q_r + Q_i + 1} \sqrt{\frac{Q_i + 1}{2Q_i^2 + 2Q_rQ_i + 3Q_i + 2Q_r + 1}}. \quad (\text{A.17})$$

$$\mathbb{E}[\sigma(\lambda)\sigma'(\lambda)\lambda_r] = \frac{2}{\pi} \frac{Q_r}{Q_r + Q_i + 1} \sqrt{\frac{Q_i + 1}{2Q_i^2 + 2Q_rQ_i + 3Q_i + 2Q_r + 1}}. \quad (\text{A.18})$$

$$\mathbb{E}[\sigma(\lambda)\sigma'(\lambda)\lambda_i] = \frac{2}{\pi} \frac{Q_i}{Q_r + Q_i + 1} \sqrt{\frac{Q_r + 1}{2Q_i^2 + 2Q_rQ_i + 3Q_i + 2Q_r + 1}}. \quad (\text{A.19})$$

$$\mathbb{E}[\phi(\rho)^2\sigma'(\lambda)^2] = \frac{2}{\pi} \frac{1}{\sqrt{2Q_r + 2Q_i + 1}}. \quad (\text{A.20})$$

$$\mathbb{E}[\sigma(\lambda)^2\sigma'(\lambda)^2] = \frac{4}{\pi^2} \frac{1}{\sqrt{1 + 2(Q_r + Q_i)}} \sin^{-1} \left( \frac{Q_r + Q_i}{1 + 3(Q_r + Q_i)} \right). \quad (\text{A.21})$$

$$\mathbb{E}[\phi(\rho)\sigma(\lambda)\sigma'(\lambda)^2] = \frac{4}{\pi^2} \frac{1}{\sqrt{2(Q_r + Q_i) + 1}} \sin^{-1} \left( \frac{R\sqrt{Q_r + Q_i}}{\sqrt{3(Q_r + Q_i) + 1} \sqrt{(2Q_r + 2Q_i + 1)[T(Q_r + Q_i) - R^2] + R^2}} \right). \quad (\text{A.22})$$

Finally, we can substitute those equations into the Eqs. (A.10-A.12) and obtained the state evolution equations used in the main Sec. 3:

$$\begin{aligned} f_{Q_r}(Q_r[k], Q_i[k], R[k], T) &= (1 - \eta\gamma)^2 Q_r[k] + \frac{4\eta(1 - \eta\gamma)}{N\pi(Q_r[k] + \Delta Q_i[k] + 1)} \times \\ &\left[ \frac{R[k](\Delta Q_i[k] + 1)}{\sqrt{T(Q_r[k] + \Delta Q_i[k] + 1) + R[k]^2}} - \frac{Q_r[k]}{\sqrt{2Q_r[k] + 2\Delta Q_i[k] + 1}} \right] \\ &+ \frac{4}{\pi^2} \frac{\rho\eta^2}{N\sqrt{2(Q_r[k] + \Delta Q_i[k]) + 1}} \left[ \frac{\pi}{2} + \sin^{-1} \left( \frac{Q_r[k] + \Delta Q_i[k]}{1 + 3(Q_r[k] + \Delta Q_i[k])} \right) + \right. \\ &\left. - 2 \sin^{-1} \left( \frac{R[k]}{\sqrt{3(Q_r[k] + \Delta Q_i[k]) + 1} \sqrt{T(2Q_r[k] + 2\Delta Q_i[k] + 1) - 2R[k]^2}} \right) \right]; \end{aligned} \quad (\text{A.23})$$

$$\begin{aligned}
f_{Q_i}(Q_r[k], Q_i[k], R[k], T) = & (1 - \eta\gamma)^2 Q_i[k] - \frac{4\eta(1 - \eta\gamma)\Delta Q_i[k]}{N\pi(Q_r[k] + \Delta Q_i[k] + 1)} \times \\
& \left[ \frac{R[k]}{\sqrt{T(Q_r[k] + \Delta Q_i[k] + 1) + R[k]^2}} + \frac{1}{\sqrt{2Q_r[k] + 2\Delta Q_i[k] + 1}} \right] + \\
& + \frac{4}{\pi^2} \frac{(1 - \rho)\Delta\eta^2}{N\sqrt{2(Q_r[k] + \Delta Q_i[k] + 1)}} \left[ \frac{\pi}{2} + \sin^{-1} \left( \frac{Q_r[k] + \Delta Q_i[k]}{1 + 3(Q_r[k] + \Delta Q_i[k])} \right) + \right. \\
& \left. - 2 \sin^{-1} \left( \frac{R[k]}{\sqrt{3(Q_r[k] + \Delta Q_i[k]) + 1} \sqrt{T(2Q_r[k] + 2\Delta Q_i[k] + 1) - 2R[k]^2}} \right) \right];
\end{aligned} \tag{A.24}$$

$$\begin{aligned}
f_R(Q_r[k], Q_i[k], R[k], T) = & (1 - \eta\gamma)R[k] + \frac{2\eta}{N\pi(Q_r[k] + \Delta Q_i[k] + 1)} \times \\
& \left[ \frac{T(Q_r[k] + \Delta Q_i[k] + 1) - R[k]^2}{\sqrt{T(Q_r[k] + \Delta Q_i[k] + 1) - R[k]^2}} - \frac{R[k]}{\sqrt{2Q_r[k] + 2\Delta Q_i[k] + 1}} \right].
\end{aligned} \tag{A.25}$$

**Elastic coupling** The introduction of the elastic coupling between stages of learning adds five new order parameters: three of them are just reminder of the previous stage and do not need to be updated  $\tilde{Q}_r = \mathbf{W}_1^r \cdot \mathbf{W}_1^r / N$ ,  $\tilde{Q}_i = \mathbf{W}_1^i \cdot \mathbf{W}_1^i / N$ , and  $\tilde{R} = \mathbf{W}_1^i \cdot \mathbf{W}^T / N$ ; two measure the correlation between the two stages  $S_r = \mathbf{W}_1^r \cdot \mathbf{W}_2^r / N$  and  $S_i = \mathbf{W}_1^i \cdot \mathbf{W}_2^i / N$  to the equations. These terms have associated their own state evolution equations slightly modified the updates of the other order parameters.

$$\begin{aligned}
Q_r[k+1] = & (1 - \eta\gamma + \eta\gamma_{12})^2 Q_r[k] + \frac{2\eta}{N} (1 - \eta\gamma + \eta\gamma_{12}) \mathbb{E}[\delta \sigma'(\lambda_r + \lambda_i) \lambda_r] \\
& + \rho \Delta \frac{\eta^2}{N} \mathbb{E}[\delta^2 \sigma'(\lambda_r + \lambda_i)^2] + 2\eta\gamma_{12}(1 - \eta\gamma + \eta\gamma_{12}) S_r[k] + \eta^2 \gamma_{12}^2 \tilde{Q}_r[k] \\
& - \frac{2\eta^2 \gamma_{12}}{N} \mathbb{E}[\delta \sigma'(\lambda_r + \lambda_i) \tilde{\lambda}_r];
\end{aligned} \tag{A.26}$$

$$\begin{aligned}
Q_i[k+1] = & (1 - \eta\gamma + \eta\gamma_{12})^2 Q_i[k] + \frac{2\eta}{N} (1 - \eta\gamma + \eta\gamma_{12}) \mathbb{E}[\delta \sigma'(\lambda_r + \lambda_i) \lambda_i] \\
& + (1 - \rho) \Delta \frac{\eta^2}{N} \mathbb{E}[\delta^2 \sigma'(\lambda_r + \lambda_i)^2] + 2\eta\gamma_{12}(1 - \eta\gamma + \eta\gamma_{12}) S_i[k] \\
& + \eta^2 \gamma_{12}^2 \tilde{Q}_i[k] - \frac{2\eta^2 \gamma_{12}}{N} \mathbb{E}[\delta \sigma'(\lambda_r + \lambda_i) \tilde{\lambda}_i];
\end{aligned} \tag{A.27}$$

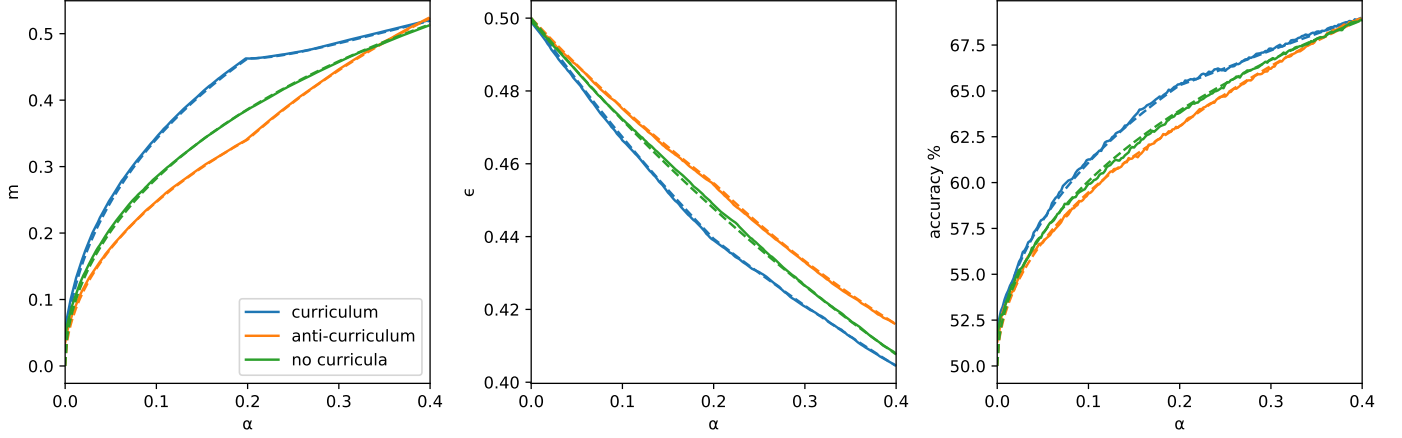
$$R[k+1] = (1 - \eta\gamma + \eta\gamma_{12})R[k] + \frac{\eta}{N} \mathbb{E}[\delta \sigma'(\lambda_r + \lambda_i) \rho] - \eta\gamma_{12} \tilde{R}[k]; \tag{A.28}$$

$$S_r[k+1] = (1 - \eta\gamma + \eta\gamma_{12})S_r[k] + \frac{\eta}{N} \mathbb{E}[\delta \sigma'(\lambda_r + \lambda_i) \tilde{\lambda}_r] - \eta\gamma_{12} \tilde{Q}_r[k]; \tag{A.29}$$

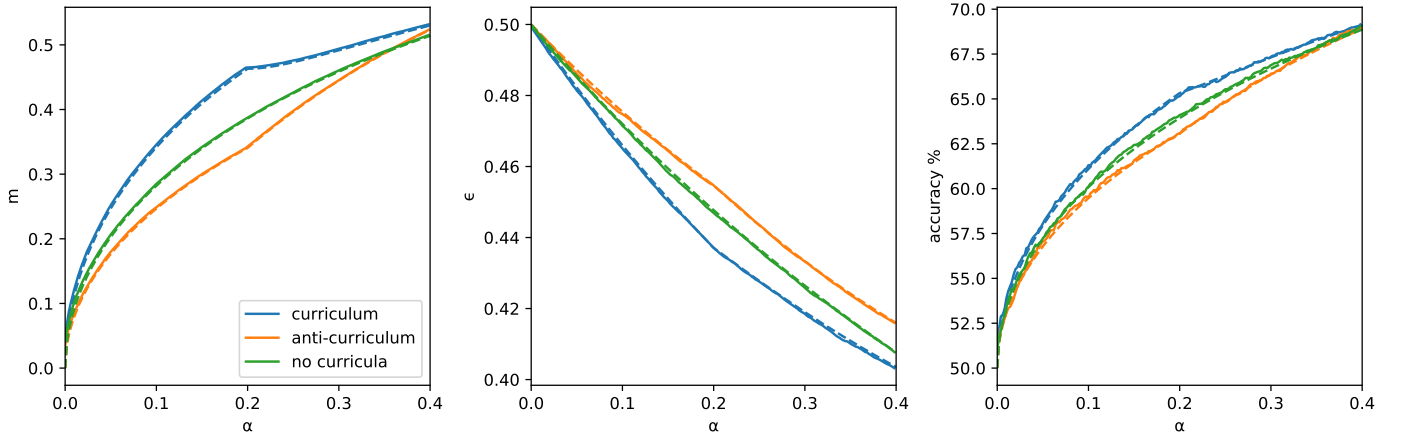
$$S_i[k+1] = (1 - \eta\gamma + \eta\gamma_{12})S_i[k] + \frac{\eta}{N} \mathbb{E}[\delta \sigma'(\lambda_r + \lambda_i) \tilde{\lambda}_i] - \eta\gamma_{12} \tilde{Q}_i[k]. \tag{A.30}$$

Introduced  $\tilde{\lambda}_r = \frac{1}{\sqrt{N}} \mathbf{x}_r \cdot \tilde{\mathbf{W}}_r$  and  $\tilde{\lambda}_i = \frac{1}{\sqrt{N}} \mathbf{x}_i \cdot \tilde{\mathbf{W}}_i$ , this two additional random variables need to be averaged together with the others. The joint distribution of  $\lambda_r, \lambda_i, \tilde{\lambda}_r, \tilde{\lambda}_i, \rho$  is still Gaussian with zero mean and covariance

$$\Sigma_{\lambda_r, \lambda_i, \tilde{\lambda}_r, \tilde{\lambda}_i, \rho} = \begin{pmatrix} Q_r & 0 & \tilde{S}_r & 0 & R \\ 0 & Q_i & 0 & \tilde{S}_i & 0 \\ \tilde{S}_r & 0 & \tilde{Q}_r & 0 & \tilde{R} \\ 0 & \tilde{S}_i & 0 & \tilde{Q}_i & 0 \\ R & 0 & \tilde{R} & 0 & T \end{pmatrix}.$$



(a) No elastic coupling.



(b) Optimal elastic coupling.

Figure A.1: **Effect of elastic coupling in the curriculum.** Figures showing the teacher-student cosine, the validation loss, and the accuracy of the three learning strategies. The two figures show the performance in presence (above) and absence (below) of elastic coupling. The dashed lines are obtained from the theoretical analysis, the full line come from the average of 500 simulations. The parameters  $\eta$ ,  $\gamma$ , initialisation are set to the optimal values for each protocol. Parameters:  $\rho = 0.5$ ,  $\alpha_1 = 0.2$ ,  $\alpha_2 = 0.2$ ,  $\Delta_1 = 0$ ,  $\Delta_2 = 1$ .

Notice that, a part from a slight change of the existing equations, the coupling introduces only two additional integrals  $\mathbb{E}[\delta \sigma'(\lambda_r + \lambda_i) \tilde{\lambda}_r]$  and  $\mathbb{E}[\delta \sigma'(\lambda_r + \lambda_i) \tilde{\lambda}_i]$ . After long, but straightforward, computations we obtain

$$\begin{aligned} \mathbb{E}[\delta \sigma'(\lambda_r + \lambda_i) \tilde{\lambda}_r] &= \frac{2}{\pi} \frac{S_r}{Q_r + Q_i + 1} \frac{Q_i + 1}{2Q_i^2 + 2Q_r Q_i + 3Q_i + 2Q_r + 1} + \\ &\quad - \frac{2TS_r - R\tilde{R}}{\pi} \frac{R(Q_i + 1)}{Q_r T - R^2} \frac{1}{Q_r + Q_i + 1} \frac{1}{\sqrt{T(Q_r + Q_i + 1) - R^2}} + \\ &\quad - \frac{2T\tilde{R} - RS_r}{\pi} \frac{1}{Q_r T - R^2} \frac{1}{\sqrt{T(Q_r + Q_i + 1) - R^2}} \frac{1}{\frac{1}{T} + \frac{R^2}{Q_r T - R^2} \left( \frac{1}{T} - \frac{Q_i + 1}{T(Q_r + Q_i + 1) - R^2} \right)}, \end{aligned} \quad (\text{A.31})$$

$$\begin{aligned} \mathbb{E}[\delta \sigma'(\lambda_r + \lambda_i) \tilde{\lambda}_i] &= \frac{2}{\pi} \frac{S_i}{Q_r + Q_i + 1} \frac{Q_r + 1}{2Q_r^2 + 2Q_r Q_i + 3Q_r + 2Q_i + 1} + \\ &\quad - \frac{2}{\pi} \frac{S_i R}{Q_r + Q_i + 1} \frac{1}{\sqrt{T(Q_r + Q_i + 1) - R^2}}. \end{aligned} \quad (\text{A.32})$$



Finally all the expected values are known and we can obtain the analytic updates Eqs. (A.26–A.30) with the coupling. Fig. A.1a shows an instance of the problem at  $\alpha_1 = 0.2$  and  $\alpha_2 = 0.2$ , a situation that is particularly adversarial for curriculum according the phase diagram Fig. 3. This situation is treated by the introduction of Gaussian priors, Fig. A.1b, consistently with the phase diagram in Fig. 8c.

## B Replica computation for the batch case

We here the detailed replica computation employed to obtain the analytic description of curriculum learning in the batch case, in section 4. As mentioned in the main, we aim to study a coupled system, represented by the following partition function:

$$\langle Z(\mathbf{W}_2, \mathbf{W}_1; \mathcal{D}_1, \mathcal{D}_2) \rangle_{\mathbf{W}_1} = \int d\mathbf{W}_1 \frac{e^{-\beta_1 \mathcal{L}_{\gamma_1}(\mathbf{W}_1, \mathcal{D}_1)}}{Z_1(\mathbf{W}_1)} \log \int d\mathbf{W}_2 e^{-\beta_2 (\mathcal{L}_{\gamma_2}(\mathbf{W}_2, \mathcal{D}_2) + \frac{\gamma_{12}}{2} \|\mathbf{W}_2 - \mathbf{W}_1\|_2^2)}, \quad (\text{B.1})$$

where the examples  $\mathcal{D}_1, \mathcal{D}_2$  are characterised by a different variances in the irrelevant components.

This type of quantity is usually denoted as a “disordered” partition function in statistical physics jargon, meaning that it is still dependent on a given realisation of the datasets – i.e., the source of disorder in this model. We want to characterise a typical realisation of this object, in the high-dimensional limit. However, because of its long-tailed statistics, the partition function turns out not to be a self-averaging quantity, i.e. its expectation over the dataset realisations will not correspond to the typical case scenario we are after. It is instead better to focus on the computation of the associated average free-entropy:

$$\Phi = \lim_{N \rightarrow \infty} \lim_{\beta_1, \beta_2 \rightarrow \infty} \frac{1}{\beta_2 N} \langle \log \langle Z(\mathbf{W}_2, \mathbf{W}_1; \mathcal{D}_1, \mathcal{D}_2) \rangle_{\mathbf{W}_1} \rangle_{\mathcal{D}_1, \mathcal{D}_2}. \quad (\text{B.2})$$

What is immediately apparent is that we have to take the expectation of a logarithm, which is not tractable with rigorous mathematical methods. Moreover, we also have to average over the measure for  $\mathbf{W}_1$ , which is also a complicated operation.

Fortunately, replica theory offers a method for approaching this calculation [36, 37]. The idea is to exploit two separate replica tricks:

- in order to evaluate the disorder average, the logarithm can be removed by replicating the second weight configuration, i.e. introducing  $n$  identical replicas  $\{\mathbf{W}_2^a\}_{a=1}^n$ , and extrapolating the final result from the  $n \rightarrow 0$  limit. This is based on the mathematical identity  $\log x = \lim_{n \rightarrow 0} \partial_n x^n$ .
- the average over the teacher can instead be computed by introducing  $\tilde{n} - 1$  non-interacting and a single interacting replica of the first weight configuration  $\{\mathbf{w}_1^c\}_{c=1}^{\tilde{n}}$ . Thus, only the  $c = 1$  replica will enter the Gaussian prior in the student measure. The sought statistical average is again recovered in the limit  $\tilde{n} \rightarrow 0$ .

Because of the high-dimensional limit we are considering, all typical realisations of the teacher vector with a given sparsity  $\rho$  will yield an identical free-entropy. Thus, we can avoid averaging and instead fix a gauge  $\mathbf{W}_{T,i} = 1$  for  $i = 1, \dots, \rho N$  and  $\mathbf{W}_{T,i} = 0$  elsewhere. In order to simplify the presentation, in the following we will assume that the datasets contain respectively  $\alpha_1$  and  $\alpha_2$  patterns, and that a curriculum ordering was employed,  $\Delta_1 < \Delta_2$ . Moreover, to avoid confusion with component and replica indices, we will denote with  $\tilde{\mathbf{W}} = \mathbf{W}_1$  and  $\mathbf{W} = \mathbf{W}_2$ , so that all quantities with a tilde refer to the optimisation on the first dataset.

After the described replication procedures, we get the following expression for the average free-entropy:

$$\Phi = \frac{1}{N} \lim_{n, \tilde{n} \rightarrow 0} \partial_n \left\langle \lim_{\tilde{\beta}, \beta \rightarrow \infty} \frac{1}{\beta} \int \prod_{c=1}^{\tilde{n}} d\tilde{\mathbf{W}}^c e^{-\frac{\tilde{\beta} \gamma_1}{2} \|\tilde{\mathbf{W}}^c\|_2^2} \prod_{\mu=1}^{\alpha_1 N} \prod_{c=1}^{\tilde{n}} e^{-\frac{\beta}{2} \ell \left( \text{sign} \left( \sum_{i=1}^{\rho N} \frac{x_i^\mu}{\sqrt{N}} \right), \sigma \left( \sum_{i=1}^N \frac{\tilde{W}_i^c x_i^\mu (\Delta_1)}{\sqrt{N}} \right) \right)} \right\rangle_{\{\mathbf{x}^\mu\}} \times \int \prod_{a=1}^n d\mathbf{W}^a e^{-\frac{\beta \gamma_2}{2} \|\mathbf{W}^a\|_2^2} e^{-\frac{\beta \gamma_{12}}{2} \|\mathbf{W}^a - \tilde{\mathbf{W}}^1\|_2^2} \prod_{\mu=1}^{\alpha_2} \prod_a e^{-\frac{\beta}{2} \ell \left( \text{sign} \left( \sum_{i=1}^{\rho N} \frac{x_i^\mu}{\sqrt{N}} \right), \sigma \left( \sum_{i=1}^N \frac{W_i^a x_i^\mu (\Delta_2)}{\sqrt{N}} \right) \right)} \right\rangle_{\{\mathbf{x}^\mu\}}, \quad (\text{B.3})$$

where  $\ell(y, \hat{y}) = \log(1 + e^{-y\hat{y}})$  indicates the standard logistic loss. The next step is to explicitly compute the averages over the dataset realisations. Before doing that, we need to isolate the dependence of our expression on the patterns, and we achieve this by introducing Dirac's  $\delta$ -functions for the pre-activations. We will use the integral representation of the  $\delta$ , with integration variables  $u$  for the teacher preactivations  $\lambda$  for the student preactivations:

$$\begin{aligned} & \frac{1}{N} \lim_{n, \tilde{n} \rightarrow 0} \partial_n \int \prod_{c=1}^{\tilde{n}} d\tilde{\mathbf{W}}^c e^{-\frac{\beta\lambda}{2} \|\tilde{\mathbf{W}}^c\|_2^2} \int \prod_{a=1}^{\tilde{n}} d\mathbf{W}^a e^{-\frac{\beta\lambda}{2} \|\mathbf{W}^a\|_2^2} e^{-\frac{\beta\lambda_{12}}{2} \|\mathbf{W}^a - \tilde{\mathbf{W}}^1\|_2^2} \\ & \times \left\langle \int \prod_{\mu} \frac{d\tilde{u}_{1\mu} d\hat{u}_{1\mu}}{2\pi} e^{i\tilde{u}_{1\mu} \left( \tilde{u}_{1\mu} - \sum_{i=1}^{\rho N} \frac{(\tilde{x}_1)_i^\mu}{\sqrt{N}} \right)} \int \prod_{\mu, c} \frac{d\tilde{\lambda}_{1\mu}^c d\hat{\lambda}_{1\mu}^c}{2\pi} e^{i\hat{\lambda}_{1\mu}^c \left( \lambda_{1\mu}^c - \sum_{i=1}^N \frac{\tilde{W}_i^c (\tilde{x}_1)_i^\mu}{\sqrt{N}} \right)} \right. \\ & \times \left. \int \prod_{\mu} \frac{du_{2\mu} d\hat{u}_{2\mu}}{2\pi} e^{i\hat{u}_{2\mu} \left( u_{2\mu} - \sum_{i=1}^{\rho N} \frac{(x_2)_i^\mu}{\sqrt{N}} \right)} \int \prod_{\mu, a} \frac{d\lambda_{2\mu}^a d\hat{\lambda}_{2\mu}^a}{2\pi} e^{i\hat{\lambda}_{2\mu}^a \left( \lambda_{2\mu}^a - \sum_{i=1}^N \frac{W_i^a (x_2)_i^\mu}{\sqrt{N}} \right)} \right\rangle_{\{\mathbf{x}^\mu\}} \\ & \times \prod_{\mu, c} e^{-\frac{\beta}{2} \ell(\text{sign}(\tilde{u}_{1\mu}), \sigma(\tilde{\lambda}_{1\mu}^c))} \prod_{\mu, a} e^{-\frac{\beta}{2} \ell(\text{sign}(u_{2\mu}), \sigma(\lambda_{2\mu}^a))}. \end{aligned} \quad (\text{B.4})$$

Thus, the disorder average is now factorised and only involves exponential terms. Since the two datasets are independent now that we made the teacher explicit, we can take the averages over each one separately. In both cases we get:

$$\begin{aligned} \langle . \rangle &= \prod_{i=1}^{\rho N} \mathbb{E}_{(x_{rel})_i^\mu} e^{-i \left( \frac{\hat{u}}{\sqrt{N}} + \sum_a \hat{\lambda}_a^\mu \frac{W_i^a}{\sqrt{N}} \right) (x_{rel})_i^\mu} \prod_{i=\rho N+1}^N \mathbb{E}_{(x_{irr})_i^\mu} e^{-i \left( \sum_a \hat{\lambda}_a^\mu \frac{W_i^a}{\sqrt{N}} \right) (x_{irr})_i^\mu} \\ &= \prod_{i=1}^{\rho N} \left( 1 - i \left( \frac{\hat{u}}{\sqrt{N}} + \sum_a \hat{\lambda}_a^\mu \frac{W_i^a}{\sqrt{N}} \right) \overline{x_{rel}} - \frac{1}{2} \left( \frac{\hat{u}}{\sqrt{N}} + \sum_a \hat{\lambda}_a^\mu \frac{W_i^a}{\sqrt{N}} \right)^2 \text{Var}(x_{rel}) \right) \\ & \times \prod_{i=\rho N+1}^N \left( 1 - i \sum_a \hat{\lambda}_a^\mu \frac{W_i^a}{\sqrt{N}} \overline{x_{irr}} - \frac{1}{2} \left( \sum_a \hat{\lambda}_a^\mu \frac{W_i^a}{\sqrt{N}} \right)^2 \text{Var}(x_{irr}) \right) \end{aligned} \quad (\text{B.5})$$

$$\begin{aligned} &= \prod_{i=1}^{\rho N} \left( 1 - \frac{1}{2N} (\hat{u}^\mu)^2 - \frac{1}{N} \sum_a \hat{u}^\mu \hat{\lambda}_a^\mu W_i^a - \frac{1}{2N} \sum_{ab} \hat{\lambda}_a^\mu \hat{\lambda}_b^\mu W_i^a W_i^b \right) \prod_{i=\rho N+1}^N \left( 1 - \frac{\Delta^\mu}{2N} \sum_{ab} \hat{\lambda}_a^\mu \hat{\lambda}_b^\mu W_i^a W_i^b \right) \\ &= e^{-\frac{1}{2} \sum_{ab} \hat{\lambda}_a^\mu \hat{\lambda}_b^\mu \left( \frac{\sum_{i=1}^{\rho N} W_i^a W_i^b}{N} + \Delta \frac{\sum_{i=\rho N+1}^N W_i^a W_i^b}{N} \right) - \frac{\rho}{2} (\hat{u}^\mu)^2 - \hat{u}^\mu \sum_a \hat{\lambda}_a^\mu \frac{\sum_{i=1}^{\rho N} W_i^a}{N}}. \end{aligned} \quad (\text{B.6})$$

This expression suggests what are the order parameters that capture the interactions of the model, namely:

- the teacher-student overlap at the end of the first learning phase:  $\tilde{R}^c = \frac{\sum_{i=1}^{\rho N} \tilde{W}_i^c}{N}$ .
- the teacher-student overlap at the end of the second learning phase:  $R^a = \frac{\sum_{i=1}^{\rho N} W_i^a}{N}$ .
- the norm of the student after the first stage, decomposed into relevant/irrelevant parts:  $\tilde{Q}_r^{cd} = \frac{\sum_{i=1}^{\rho N} \tilde{W}_i^c \tilde{W}_i^d}{N}$ ,  
 $\tilde{Q}_i^{cd} = \frac{\sum_{i=\rho N+1}^N \tilde{W}_i^c \tilde{W}_i^d}{N}$
- the norm of the student after the second stage, decomposed into relevant/irrelevant parts:  $Q_r^{ab} = \frac{\sum_{i=1}^{\rho N} W_i^a W_i^b}{N}$ ,  
 $Q_i^{ab} = \frac{\sum_{i=\rho N+1}^N W_i^a W_i^b}{N}$

Therefore, after introducing these definitions by means of Dirac's  $\delta$ -functions, we can rewrite our replicated expression as:

$$\Omega^n = \int \prod_c \frac{d\tilde{R}^c d\hat{\tilde{R}}^c}{2\pi/N} \int \prod_a \frac{dR^a d\hat{R}^a}{2\pi/N} \int \prod_{cd} \frac{d\tilde{Q}_r^{cd} d\hat{\tilde{Q}}_r^{cd}}{2\pi/N} \int \prod_{cd} \frac{d\tilde{Q}_i^{cd} d\hat{\tilde{Q}}_i^{cd}}{2\pi/N} \int \prod_{ab} \frac{dQ_r^{ab} d\hat{Q}_r^{ab}}{2\pi/N} \int \prod_{ab} \frac{dQ_i^{ab} d\hat{Q}_i^{ab}}{2\pi/N}$$

$$\times G_i G_S \left( \hat{\tilde{R}}, \hat{R}, \hat{\tilde{Q}}_r, \hat{Q}_r \right)^{\rho N} G_S \left( 0, 0, \tilde{Q}_i, Q_i \right)^{(1-\rho)N} G_E \left( \Delta_1, \tilde{Q}_r, \tilde{Q}_i, \tilde{R}, \tilde{n} \right)^{\alpha_1 N} G_E \left( \Delta_2, Q_r, Q_i, R, n \right)^{\alpha_2 N} \quad (\text{B.7})$$

Where we introduced interaction, entropic and energetic potentials:

$$G_i = \exp \left( -N \left( \sum_c \hat{\tilde{m}}^c \tilde{m}^c + \sum_a \hat{m}^a m^a + \sum_{cd} \hat{\tilde{Q}}^{cd} \tilde{Q}_r^{cd} + \sum_{cd} \hat{\tilde{Q}}^{cd} \tilde{Q}_i^{cd} + \sum_{ab} \hat{Q}_r^{ab} Q_r^{ab} + \sum_{ab} \hat{Q}_i^{ab} Q_i^{ab} \right) \right) \quad (\text{B.8})$$

$$G_S \left( \tilde{R}, R, \tilde{Q}, Q \right) = \int \prod_c \left[ d\tilde{W}^c e^{-\frac{\beta\gamma}{2} (\tilde{W}^c)^2} \right] e^{-\frac{n\beta\gamma_{12}}{2} (\tilde{W}^1)^2} \int \prod_a \left[ dW^a e^{-\frac{\beta(\gamma+\gamma_{12})}{2} (W^a)^2} \right] \quad (\text{B.9})$$

$$\begin{aligned} & \times \exp \left( \sum_c \hat{\tilde{R}}^c \tilde{W}^c + \sum_a \hat{R}^a W^a + \sum_{cd} \hat{\tilde{Q}}^{cd} \tilde{W}^c \tilde{W}^d + \sum_{ab} \hat{Q}^{ab} W^a W^b + \beta\gamma_{12} W^a \tilde{W}^1 \right) \\ G_E \left( \Delta, Q_r, Q_i, m, n \right) &= \int \frac{dud\hat{u}}{2\pi} e^{iu\hat{u}} e^{-\frac{\rho}{2}(\hat{u})^2} \int \prod_{a=1}^n \frac{d\lambda^a d\hat{\lambda}^a}{2\pi} e^{i\lambda^a \hat{\lambda}^a} \\ & \times e^{-\frac{1}{2} \sum_{ab} \hat{\lambda}_a \hat{\lambda}_b (Q_r^{ab} + \Delta Q_i^{ab}) - \hat{u} \sum_a \hat{\lambda}_a R^a - \frac{\beta}{2} \ell(u, \lambda^a)} \end{aligned} \quad (\text{B.10})$$

### Replica Symmetric Ansatz

The replica trick allowed us to express the average free-entropy as a function of the overlap order parameters. However, these objects are  $n \times n$  matrices or  $n$ -dimensional vectors and in principle we have to average over all their possible realisations. Fortunately, the integrand function is exponential in  $N$  and in the thermodynamic limit  $N \rightarrow \infty$  the integrals are dominated by the extremisers of the action, and thus can be approximated with the saddle-point method. Still, we need a guess for how to parametrise these order parameters. The simplest possible ansatz, which turns out to be the correct one in convex problems as the one at hand, is the so-called Replica Symmetric ansatz, given by:

- $\tilde{R}^c = \tilde{R}$
- $R^a = R$
- $\tilde{Q}_{r/i}^{cd} = \tilde{q}_{r/i}$ , for  $c \neq d$ ;  $\tilde{Q}_{r/i}^{cd} = \tilde{Q}_{r/i}$  for  $c = d$ .
- $Q_{r/n}^{ab} = q_{r/n}$  for  $a \neq b$ ;  $Q_{r/n}^{ab} = Q_{r/n}$  for  $a = b$ .

We also perform a Wick rotation  $-i\hat{Q}_{ac,bd} \rightarrow \hat{Q}_{ac,bd}$  in order to deal with real valued conjugate parameters and pose a similar ansatz for them. In the next paragraph we will compute the three terms separately, and finally put them together in the expression for the RS free-entropy.

### Interaction term

We start by evaluating the interaction term, or better its normalised logarithm  $g_i = \lim_{\tilde{n} \rightarrow 0} \log G_i / (nN)$ :

$$\begin{aligned} g_i &= - \lim_{\tilde{n} \rightarrow 0} \frac{1}{n} \left( \tilde{n} \hat{\tilde{R}} \tilde{R} + n \hat{R} R + \tilde{n} \left( \frac{\hat{\tilde{Q}}_r \tilde{Q}_r}{2} + \frac{\hat{\tilde{Q}}_i \tilde{Q}_i}{2} \right) + \frac{\tilde{n}(\tilde{n}-1)}{2} (\hat{\tilde{q}}_r \tilde{q}_r + \hat{\tilde{q}}_i \tilde{q}_i) \right. \\ & \quad \left. + n \left( \frac{\hat{Q}_r Q_r}{2} + \frac{\hat{Q}_i Q_i}{2} \right) + \frac{n(n-1)}{2} (\hat{q}_r q_r + \hat{q}_i q_i) \right) \end{aligned} \quad (\text{B.11})$$

$$= - \left( \hat{R} R + \frac{(\hat{Q}_r Q_r + \hat{Q}_i Q_i)}{2} - \frac{1}{2} (\hat{q}_r q_r + \hat{q}_i q_i) \right) \quad (\text{B.12})$$

In order to recover the optimisation problems entailed in the curriculum procedure, we now have to consider the zero temperature limit of this expression. When  $\beta \rightarrow \infty$ , the order parameters follow non-trivial scaling laws:

- $\hat{Q} \rightarrow \beta^2 \hat{Q} + \mathcal{O}(\beta)$ ,  $\hat{q} \rightarrow \beta^2 \hat{Q}$
- $(\hat{Q} - \hat{q}) \rightarrow -\beta \delta \hat{Q}$
- $\hat{R} \rightarrow \beta \hat{R}$
- $Q - q = \delta Q / \beta$

and similarly for the tilde parameters. Intuitively, looking at the last scaling law, we see that as the measure gets focused on the single minimiser of the loss, the overlap between different replicas  $q$  rapidly converges to the norm  $Q$ . Moreover, the scaling with the inverse temperature of the conjugate parameters prevents the interaction term from becoming sub-dominant in the saddle-point. If we substitute the rescaled parameters in the above expression we obtain:

$$g_i = -\beta \left( \hat{R} R + \frac{1}{2} \left( \hat{Q}_r \delta Q_r - \delta \hat{Q}_r Q_r \right) + \frac{1}{2} \left( \hat{Q}_i \delta Q_i - \delta \hat{Q}_i Q_i \right) \right) \quad (\text{B.13})$$

### Entropic term

We can now compute a similar quantity for the entropic potential,  $g_i = \lim_{n \rightarrow 0} \frac{1}{n} \log G_S(\tilde{R}, R, \tilde{Q}, Q)$ . The general expression we will obtain can be specialised to the two cases  $\left( \left\{ \tilde{R}, R, \tilde{Q}_r, Q_r \right\}, \left\{ 0, 0, \tilde{Q}_i, Q_i \right\} \right)$  appearing in the free-entropy. After substituting the RS ansatz we find:

$$\begin{aligned} g_S &= \lim_{n \rightarrow 0} \frac{1}{n} \log \int \prod_c \left[ d\tilde{W}^c e^{-\frac{\beta\gamma}{2} (\tilde{W}^c)^2} \right] e^{-\frac{n\beta\gamma_{12}}{2} (\tilde{W}^1)^2} \int \prod_a \left[ dW^a e^{-\frac{\beta(\gamma+\gamma_{12})}{2} (W^a)^2} \right] \\ &\quad \times \exp \left( \hat{R} \sum_c \tilde{W}^c + \hat{R} \sum_a W^a + \frac{1}{2} (\hat{Q} - \hat{q}) \sum_c (\tilde{W}^c)^2 + \frac{\hat{q}}{2} \left( \sum_c \tilde{W}^c \right)^2 + \right. \\ &\quad \left. + \frac{1}{2} (\hat{Q} - \hat{q}) \sum_a (W^a)^2 + \frac{\hat{q}}{2} \left( \sum_a W^a \right)^2 + \beta\gamma_{12} \sum_a \tilde{W}^1 W^a \right) \\ &= \lim_{n \rightarrow 0} \frac{1}{n} \log \int \mathcal{D}z \int \mathcal{D}\tilde{z} \int \prod_c \left[ d\tilde{W}^c e^{-\frac{\beta\gamma}{2} (\tilde{W}^c)^2} \right] e^{-\frac{n\beta\gamma_{12}}{2} (\tilde{W}^1)^2} \int \prod_a dW^a e^{-\frac{\beta(\gamma+\gamma_{12})}{2} (W^a)^2} \\ &\quad \times \exp \left( \frac{1}{2} (\hat{Q} - \hat{q}) \sum_c (\tilde{W}^c)^2 + \frac{1}{2} (\hat{Q} - \hat{q}) \sum_a (W^a)^2 + \right. \\ &\quad \left. + \left( \hat{R} + \sqrt{\hat{q}\tilde{z}} \right) \sum_c \tilde{W}^c + \left( \hat{R} + \beta\gamma_{12} W_1 + \sqrt{\hat{q}z} \right) \sum_a W^a \right) \\ &= \int \mathcal{D}z \int \mathcal{D}\tilde{z} \frac{\int d\tilde{W} e^{-\frac{1}{2}(\beta\tilde{\gamma} - (\hat{Q} - \hat{q}))\tilde{W}^2 + (\hat{R} + \sqrt{\hat{q}\tilde{z}})\tilde{W}} \log \left( \int dW e^{-\frac{1}{2}(\beta(\gamma+\gamma_{12}) - (\hat{Q} - \hat{q}))W^2 + (\hat{R} + \beta\gamma_{12}W_1 + \sqrt{\hat{q}z})W} \right)}{\int d\tilde{W} e^{-\frac{1}{2}(\beta\tilde{\gamma} - (\hat{Q} - \hat{q}))\tilde{W}^2 + (\hat{R} + \sqrt{\hat{q}\tilde{z}})\tilde{W}}} \quad (\text{B.15}) \end{aligned}$$

In the zero-temperature limit, we consider the same rescaling of the order parameters we described above. The integrals over the weights become an extremum operation:

$$g_s = \lim_{\beta \rightarrow \infty} \beta \int \mathcal{D}z \int \mathcal{D}\tilde{z} M_s^*, \quad (\text{B.16})$$

where:

$$M_s^* = \max_W \left\{ -\frac{1}{2} \left( (\gamma + \gamma_{12}) + \delta \hat{Q} \right) W^2 + \left( \hat{R} + \gamma_{12} \tilde{W}^* + \sqrt{\hat{Q}\tilde{z}} \right) W \right\} \quad (\text{B.17})$$

$$= \frac{1}{2} \frac{\left( \hat{R} + \gamma_{12} \tilde{W}^* + \sqrt{\hat{Q}} z \right)^2}{(\gamma + \gamma_{12}) + \delta \hat{Q}} \quad (\text{B.18})$$

and where:  $\tilde{W}^* = \operatorname{argmax}_{\tilde{W}} \left\{ -\frac{1}{2}(\tilde{\gamma} + \delta \hat{\tilde{Q}}) \tilde{W}^2 + (\hat{R} + \sqrt{\hat{\tilde{Q}}} \tilde{z}) \tilde{W} \right\} = \frac{\hat{R} + \sqrt{\hat{\tilde{Q}}} \tilde{z}}{\tilde{\gamma} + \delta \hat{\tilde{Q}}}$ .

Finally also the  $\int \mathcal{D}z \int \mathcal{D}\tilde{z}$  integrations can be carried out, giving:

$$\beta \int \mathcal{D}z \int \mathcal{D}\tilde{z} M_s^* = \beta \int \mathcal{D}z \int \mathcal{D}\tilde{z} \frac{1}{2} \frac{\left( \hat{R} + \gamma_{12} \frac{\hat{R} + \sqrt{\hat{\tilde{Q}}} \tilde{z}}{\tilde{\gamma} + \delta \hat{\tilde{Q}}} + \sqrt{\hat{Q}} z \right)^2}{(\gamma + \gamma_{12}) + \delta \hat{Q}} \quad (\text{B.19})$$

$$= \frac{\beta}{2} \frac{\left( \hat{R} + \frac{\hat{R} \gamma_{12}}{\tilde{\gamma} + \delta \hat{\tilde{Q}}} \right)^2 + \left( \frac{\gamma_{12} \sqrt{\hat{\tilde{Q}}}}{\tilde{\gamma} + \delta \hat{\tilde{Q}}} \right)^2 + \hat{Q}}{(\gamma + \gamma_{12}) + \delta \hat{Q}} \quad (\text{B.20})$$

So, specialising to the the two terms that appear in the free-entropy we get:

$$g_S(\gamma_1, \gamma_2, \gamma_{12}) = \rho g_s \left( \tilde{R}, R, \tilde{Q}_r, Q_r \right) + (1 - \rho) g_s \left( 0, 0, \tilde{Q}_i, Q_i \right) \quad (\text{B.21})$$

$$= \frac{\beta}{2} \left( \rho \frac{\left( \hat{R} + \frac{\hat{R} \gamma_{12}}{\gamma_1 + \delta \hat{\tilde{Q}}_r} \right)^2 + \left( \frac{\gamma_{12} \sqrt{\hat{\tilde{Q}}_r}}{\gamma_1 + \delta \hat{\tilde{Q}}_r} \right)^2 + \hat{Q}_r}{(\gamma_2 + \gamma_{12}) + \delta \hat{Q}_r} + (1 - \rho) \frac{\left( \frac{\gamma_{12} \sqrt{\hat{\tilde{Q}}_i}}{\gamma_1 + \delta \hat{\tilde{Q}}_i} \right)^2 + \hat{Q}_i}{(\gamma_2 + \gamma_{12}) + \delta \hat{Q}_i} \right)$$

## Energetic term

Since one of the two energetic terms appearing in the replicated free-energy depends on the  $\tilde{n}$  replicas of the first weight configuration, and there is no interaction, we can take the  $\tilde{n} \rightarrow 0$  limit directly. Therefore we only have to evaluate the other contribution (dependent on the  $n$  replicas of the second weight configuration). Defining  $Q = Q_r + \Delta Q_i$ ,  $\tilde{Q} = \tilde{Q}_r + \Delta \tilde{Q}_i$ , we evaluate  $g_E = \lim_{n \rightarrow 0} \frac{1}{n} \log(G_E)$  in the RS ansatz:

$$g_E = \lim_{n \rightarrow 0} \frac{1}{n} \log \int \frac{dud\hat{u}}{2\pi} e^{iu\hat{u}} e^{-\frac{\rho}{2}(\hat{u})^2} \int \prod_a \left( \frac{d\lambda^a d\hat{\lambda}^a}{2\pi} e^{i\lambda^a \hat{\lambda}^a} \right) \quad (\text{B.22})$$

$$\times e^{-\frac{1}{2}(Q-q) \sum_a (\hat{\lambda}_a)^2 - \frac{1}{2}q(\sum_a \hat{\lambda}_a)^2 - \hat{u}R \sum_a \hat{\lambda}_a - \beta \sum_a \ell(u, \lambda^a)}$$

$$= \lim_{n \rightarrow 0} \frac{1}{n} \log \int \frac{du}{\sqrt{2\pi\rho}} \int \prod_a \left( \frac{d\lambda^a d\hat{\lambda}^a}{2\pi} e^{i\lambda^a \hat{\lambda}^a} \right) \quad (\text{B.23})$$

$$\times e^{-\frac{1}{2}(Q-q) \sum_a (\hat{\lambda}_a)^2 - \frac{1}{2}q(\sum_a \hat{\lambda}_a)^2 - \beta \sum_a \ell(u, \lambda^a) - \frac{1}{2\rho}(u + iR \sum_a \hat{\lambda}_a)^2}$$

$$= \lim_{n \rightarrow 0} \frac{1}{n} \log \int \mathcal{D}z_0 \int \mathcal{D}u \left\{ \int \mathcal{D}\lambda e^{-\beta \ell \left( \sqrt{\rho} u, \sigma \left( \sqrt{(Q-q)\lambda} + \sqrt{q - \frac{m^2}{\rho}} z_0 + \frac{m}{\sqrt{\rho}} u \right) \right)} \right\}^n \quad (\text{B.24})$$

$$= \int \mathcal{D}z_0 \int \mathcal{D}u \log \int \mathcal{D}\lambda e^{-\beta \ell \left( \sqrt{\rho} u, \sigma \left( \sqrt{Q-q}\lambda + \sqrt{q - \frac{m^2}{\rho}} z_0 + \frac{m}{\sqrt{\rho}} u \right) \right)}$$

So in the  $\beta \rightarrow \infty$  limit, with the proper rescalings, we get:

$$g_E = \beta \int \mathcal{D}z \int \mathcal{D}u M_E^*, \quad (\text{B.25})$$

where:

$$M_E^* = \max_{\lambda} -\frac{\lambda^2}{2} - \ell \left( \text{sign}(\sqrt{\rho} u), \sigma \left( \sqrt{\delta Q_r + \Delta \delta Q_i} \lambda + \sqrt{Q_r + \Delta Q_i - \frac{R^2}{\rho}} z + \frac{R}{\sqrt{\rho}} u \right) \right) \quad (\text{B.26})$$

## RS Free-entropy

Finally, assuming the we can write down the RS free-entropy for the curriculum ordering as:

$$\begin{aligned} \Phi/\beta = & -\text{extr} \left( \hat{R}R + \frac{1}{2} \left( \left( \hat{Q}\delta Q - \delta\hat{Q}Q \right)_r + \left( \hat{Q}\delta Q - \delta\hat{Q}Q \right)_i \right) \right) \\ & + g_S(\gamma_1, \gamma_2, \gamma_{12}) + \alpha_2 g_E(\Delta_2), \end{aligned} \quad (\text{B.27})$$

where  $g_S$  is defined in equation (B.21) and  $g_E$  is defined in equation (B.25). The order parameters for the teacher system are obtained independently from identical equations, after substituting  $\lambda_1 \rightarrow 0, \lambda_2 \rightarrow \lambda_1$  and  $\lambda_{12} \rightarrow 0, \alpha_2 \rightarrow \alpha_1$  and  $\Delta_2 \rightarrow \Delta_1$ , and after adding a tilde to the remaining parameters.

The saddle-point equations, yielding at convergence the asymptotic prediction for the order parameters, can be found by posing stationarity conditions for the free-entropy with respect to all overlaps.

Note that, if instead of the simple setting just considered, where the data slice in the second stage has homogeneous variance for the irrelevant components, there are multiple subsets with different sizes and variances, the only variation in the free-entropy is in the energetic contribution. In general one will have a sum:

$$\sum_s \alpha_s g_E(\Delta_s) \quad (\text{B.28})$$

over each of these subsets.

Moreover, if instead of two stages we consider multiple learning stages, the free-entropy for each successive step has an identical form, and one only has to substitute the tilde parameters with the order parameters obtained at the previous step. Note that the simplicity of nesting stages in this problem is connected to the convexity of this learning setting. Generally, adding more steps would increase the complexity of the calculation considerably.

## Generalisation error

With the saddle-point values for the order parameters, one can easily evaluate the generalisation error on new datapoints, which is the measure of performance we are employing in the main. This performance can be obtained as:

$$1 - \epsilon_g = \left\langle \Theta \left( \left( \frac{\mathbf{W}_T \cdot x}{\sqrt{N}} \right) \left( \frac{\mathbf{W}_2 \cdot x}{\sqrt{N}} \right) \right) \right\rangle_{x(\Delta)} \quad (\text{B.29})$$

where  $\Delta$  is the variance of the irrelevant components for the new pattern. A shortcut for evaluating this expression is to insert the order parameters in the expression through Dirac's  $\delta$ s. After a straightforward calculation, along the same lines of the one presented above, one obtains:

$$\epsilon_g = \frac{1}{\pi} \arccos \left( \frac{R}{\sqrt{\rho(Q_r + \Delta Q_i)}} \right). \quad (\text{B.30})$$

Of course, the generalisation accuracy is just the complementary quantity  $1 - \epsilon_g$ .

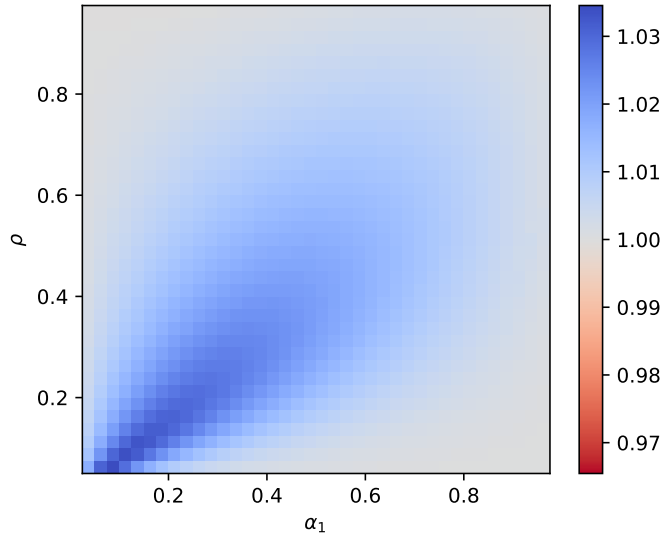


## C Impact of the sparsity level of the teacher

In the simple teacher-student problem analysed in this work, sparsity is a key ingredient, since it naturally introduces the definition of relevant and irrelevant input components, thus allowing for the study of curriculum learning strategies.

As mentioned in the main, any non-trivial setting  $0 < \rho < 1$  could in principle give rise to the same qualitative phenomenology (except, possibly, for the case of extremely low sparsity levels, which we are not investigating in the present study). However, the precise setting does have an impact on the precise regimes of sample complexities where curriculum strategies are found to be effective.

In this section, we look at the impact of sparsity in the comparison between the performance of curriculum and anti-curriculum. In particular, we consider the case of  $\Delta_1 = 0$  and  $\Delta_2 = 1$ , variable number of easy samples  $\alpha_1$  but fixed dataset size  $\alpha_1 + \alpha_2 = 1$ . Thus, the x-axis could also be interpreted as the fraction of simple patterns in the complete dataset.



(a) Curriculum learning vs anti-curriculum

**Figure C.1: Performance gap as a function of the teacher sparsity levels.** The figure shows the ratio between the accuracy reached by curriculum learning over anti-curriculum as a function of the number of easy samples in a dataset of dimension  $\alpha_1 + \alpha_2 = 1$ , and of the sparsity level of the teacher  $\rho$ . Note that  $\rho$  can also be seen as the fraction of relevant components in the inputs.  $\Delta_1 = 0$  and  $\Delta_2 = 1$ .  $\gamma_1 = \gamma_2$  and  $\gamma_{12}$  where set the values that optimise test performance. The results are obtained from the replica asymptotics in the batch setting.

In fig. C.1, we show a phase diagram that highlights the impact of sparsity in the studied model. We observe that:

- the region where curriculum learning is found to be most effective is close to the diagonal of the phase diagram, where the fraction of simple examples in the dataset is comparable to the sparsity level of the teacher, i.e. to the fraction of relevant components in the input.
- When the fraction of easy samples is much smaller than the sparsity, the slice of hard samples carries most of the information. Introducing a strong prior in the direction of the optimiser of the first (simple) stage becomes detrimental. Thus, curriculum cannot be too advantageous.
- When instead the fraction of easy patterns is larger than the sparsity, the slice of hard samples carries so little information (with respect to the easy one) that it is better to ignore it, and just learn from the simple examples. Thus, curriculum is not found to outperform anti-curriculum.

## D Simulations on CIFAR10



Figure D.1: **CIFAR10-derived real data task.** Each input consists of a task-relevant image on the left, and an irrelevant image on the right. The irrelevant image varies in contrast across columns (a)-(d), from zero to one in steps of .25.

**Task design.** Because a sparse set of relevant features is crucial to observing curriculum effects in our model, we created a task based on real data that has this property. In particular we create  $32 \times 64$  pixel input examples by concatenating two images side-by-side from the CIFAR10 dataset (Fig. D.1). The correct output label is given by the label of the image on the left, while the image on the right is an irrelevant distractor. To vary difficulty, we scale the contrast of the irrelevant image. This dataset is meant to instantiate a simple example of learning an object classification amidst clutter. We emphasise that, as in our synthetic data model, each training sample always contains the same relevant and distractor images (i.e., we are not considering a data augmentation setting where each relevant image appears with many non-relevant images). To ensure no cross-contamination of training and testing samples, the distractor images for the training and test sets are drawn only from the same set.

**Model architecture and training regime.** We train a single layer network with cross entropy loss (i.e. softmax regression), implemented in Pytorch Lightning by modifying the MIT-licensed `PyTorch_CIFAR10` repository (<https://zenodo.org/record/4431043#.YLmz6zZKhsA>) to ensure that training parameters accord with standard practice. Networks were trained with SGD and Nesterov momentum, under default parameters: a learning rate of  $1e-2$ , momentum parameter 0.9, batch size 256, and 100 epochs. The learning rate was annealed according to the ‘WarmUpCosine’ schedule used in `PyTorch_CIFAR10`, which linearly reduces the learning rate over the first 30% of training steps before switching to a cosine shaped schedule on the remainder.

**Experiment details and hyperparameter optimisation.** For the first phase of training, we used dataset sizes in 10 equal steps between 1000 and 50000. For the second phase, we used nine dataset sizes in 9 equal steps between 5333 and 48000. We optimised hyperparameters in each phase separately. In the first phase, we evaluated all combinations of initialisation scales of  $\{0, .2, .5, 1.\}$ , weight decay parameters of  $\{0, .2, .5, 1., 2.\}$ , and curriculum policy, for five random seeds. In the second phase, for each random seed and curriculum condition, we continued training from the best-performing model obtained in the first phase. We trained all combinations of five elastic penalties log spaced between  $1e-3$  and  $1e2$ , and weight decay parameters  $\{0, .2, .5.\}$ . We then compute the best performing model for each seed and take the mean over seeds. Finally, to evaluate the no-curriculum performance, we train shuffled dataset models with initialisation scales  $\{0, .2, .5, 1.\}$  and weight decay parameters

$\{0, .2, .5\}$ . For visualisation purposes, we used nearest-neighbors interpolation in the phase portrait to provide values for all points used in the synthetic experiments. Experiments were run on V100 GPUs and required approximately 10000 GPU hours (including debugging and development), or  $\approx 1110$  kg CO<sub>2</sub> eq according to the [MachineLearning Impact calculator](#) of Lacoste et al., 2019.

## References

- [1] Renee Elio and John Anderson. The effects of information order and learning mode on schema abstraction. *Memory & Cognition*, 12:20–30, January 1984.
- [2] Robert C. Wilson, Amitai Shenhav, Mark Straccia, and Jonathan D. Cohen. The Eighty Five Percent Rule for optimal learning. *Nature Communications*, 10(1):4646, November 2019.
- [3] Judith Avrahami, Yaakov Kareev, Yonatan Bogot, Ruth Caspi, Salomka Dunaevsky, and Sharon Lerner. Teaching by Examples: Implications for the Process of Category Acquisition. *The Quarterly Journal of Experimental Psychology Section A*, 50(3):586–606, August 1997. Publisher: SAGE Publications.
- [4] Harold Pashler and Michael C. Mozer. When does fading enhance perceptual category learning? *Journal of Experimental Psychology: Learning, Memory, and Cognition*, 39(4):1162–1173, 2013.
- [5] Adam N. Hornsby and Bradley C. Love. Improved classification of mammograms following idealized training. *Journal of Applied Research in Memory and Cognition*, 3(2):72–76, June 2014.
- [6] Brett D. Roads, Buyun Xu, June K. Robinson, and James W. Tanaka. The easy-to-hard training advantage with real-world medical images. *Cognitive Research: Principles and Implications*, 3, October 2018.
- [7] The International Brain Laboratory, Valeria Aguilon-Rodriguez, Dora Angelaki, Hannah Bayer, Niccolo Bonacchi, Matteo Carandini, Fanny Cazettes, Gaelle Chapuis, Anne K Churchland, Yang Dan, Eric Dewitt, Mayo Faulkner, Hamish Forrest, Laura Haetzel, Michael Häusser, Sonja B Hofer, Fei Hu, Anup Khanal, Christopher Krasniak, Ines Laranjeira, Zachary F Mainen, Guido Meijer, Nathaniel J Miska, Thomas D Mrsic-Flogel, Masayoshi Murakami, Jean-Paul Noel, Alejandro Pan-Vazquez, Cyrille Rossant, Joshua Sanders, Karolina Socha, Rebecca Terry, Anne E Urai, Hernando Vergara, Miles Wells, Christian J Wilson, Ilana B Witten, Lauren E Wool, and Anthony M Zador. Standardized and reproducible measurement of decision-making in mice. *eLife*, 10:e63711, May 2021. Publisher: eLife Sciences Publications, Ltd.
- [8] Jeffrey L. Elman. Learning and development in neural networks: the importance of starting small. *Cognition*, 48(1):71–99, July 1993.
- [9] Kai A. Krueger and Peter Dayan. Flexible shaping: how learning in small steps helps. *Cognition*, 110(3):380–394, March 2009.
- [10] Yoshua Bengio, Jérôme Louradour, Ronan Collobert, and Jason Weston. Curriculum learning. In *Proceedings of the 26th annual international conference on machine learning*, pages 41–48, 2009.
- [11] Anastasia Pentina, Viktoriia Sharmanska, and Christoph H. Lampert. Curriculum learning of multiple tasks. pages 5492–5500. IEEE Computer Society, June 2015. ISSN: 1063-6919.
- [12] Guy Hacohen and Daphna Weinshall. On the power of curriculum learning in training deep networks. In *ICML*, volume 97, pages 2535–2544. PMLR, 2019.
- [13] Xiaoxia Wu, Ethan Dyer, and Behnam Neyshabur. When do curricula work? *ICLR*, 2020.

- [14] Tom Brown, Benjamin Mann, Nick Ryder, Melanie Subbiah, Jared D. Kaplan, Prafulla Dhariwal, Arvind Neelakantan, Pranav Shyam, Girish Sastry, Amanda Askell, Sandhini Agarwal, Ariel Herbert-Voss, Gretchen Krueger, Tom Henighan, Rewon Child, Aditya Ramesh, Daniel Ziegler, Jeffrey Wu, Clemens Winter, Chris Hesse, Mark Chen, Eric Sigler, Mateusz Litwin, Scott Gray, Benjamin Chess, Jack Clark, Christopher Berner, Sam McCandlish, Alec Radford, Ilya Sutskever, and Dario Amodei. Language Models are Few-Shot Learners. *Advances in Neural Information Processing Systems*, 33:1877–1901, 2020.
- [15] Minqi Jiang, Edward Grefenstette, and Tim Rocktäschel. Prioritized Level Replay. *arXiv:2010.03934 [cs]*, January 2021. arXiv: 2010.03934.
- [16] Daphna Weinshall, Gad Cohen, and Dan Amir. Curriculum learning by transfer learning: Theory and experiments with deep networks. In *International Conference on Machine Learning*, pages 5238–5246. PMLR, 2018.
- [17] Daphna Weinshall and Dan Amir. Theory of curriculum learning, with convex loss functions. *Journal of Machine Learning Research*, 21(222):1–19, 2020.
- [18] Miguel Ruiz-García, Andrea J Liu, and Eleni Katifori. Tuning and jamming reduced to their minima. *Physical Review E*, 100(5):052608, 2019.
- [19] Marc Mézard, Giorgio Parisi, and Miguel Angel Virasoro. *Spin glass theory and beyond: An Introduction to the Replica Method and Its Applications*, volume 9. World Scientific Publishing Company, 1987.
- [20] Andreas Engel and Christian Van den Broeck. *Statistical mechanics of learning*. Cambridge University Press, 2001.
- [21] Lenka Zdeborová and Florent Krzakala. Statistical physics of inference: Thresholds and algorithms. *Advances in Physics*, 65(5):453–552, 2016.
- [22] Yasaman Bahri, Jonathan Kadmon, Jeffrey Pennington, Sam S Schoenholz, Jascha Sohl-Dickstein, and Surya Ganguli. Statistical mechanics of deep learning. *Annual Review of Condensed Matter Physics*, 2020.
- [23] Leticia F Cugliandolo and Jorge Kurchan. Analytical solution of the off-equilibrium dynamics of a long-range spin-glass model. *Physical Review Letters*, 71(1):173, 1993.
- [24] Michael Biehl and Holm Schwarze. Learning by on-line gradient descent. *Journal of Physics A: Mathematical and general*, 28(3):643, 1995.
- [25] M.S. Advani, A.M. Saxe, and H. Sompolinsky. High-dimensional dynamics of generalization error in neural networks. *Neural Networks*, 132:428 – 446, 2020.
- [26] Sebastian Goldt, Madhu Advani, Andrew M Saxe, Florent Krzakala, and Lenka Zdeborová. Dynamics of stochastic gradient descent for two-layer neural networks in the teacher-student setup. In H. Wallach, H. Larochelle, A. Beygelzimer, F. d'Alché-Buc, E. Fox, and R. Garnett, editors, *Advances in Neural Information Processing Systems*, volume 32. Curran Associates, Inc., 2019.
- [27] Stefano Sarao Mannelli, Florent Krzakala, Pierfrancesco Urbani, and Lenka Zdeborova. Passed & spurious: Descent algorithms and local minima in spiked matrix-tensor models. 97:4333–4342, 09–15 Jun 2019.
- [28] Stefano Sarao Mannelli, Giulio Biroli, Chiara Cammarota, Florent Krzakala, and Lenka Zdeborová. Who is afraid of big bad minima? analysis of gradient-flow in spiked matrix-tensor models. In *Advances in Neural Information Processing Systems*, pages 8679–8689, 2019.
- [29] Stefano Sarao Mannelli, Giulio Biroli, Chiara Cammarota, Florent Krzakala, Pierfrancesco Urbani, and Lenka Zdeborová. Complex dynamics in simple neural networks: Understanding gradient flow in phase retrieval. 33:3265–3274, 2020.

- [30] Hugo Cui, Luca Saglietti, and Lenka Zdeborová. Large deviations for the perceptron model and consequences for active learning. In *Mathematical and Scientific Machine Learning*, pages 390–430. PMLR, 2020.
- [31] David Saad and Sara A Solla. Exact solution for on-line learning in multilayer neural networks. *Physical Review Letters*, 74(21):4337, 1995.
- [32] Tom Kocmi and Ondřej Bojar. Curriculum Learning and Minibatch Bucketing in Neural Machine Translation. In *Proceedings of the International Conference Recent Advances in Natural Language Processing, RANLP 2017*, pages 379–386, Varna, Bulgaria, September 2017. INCOMA Ltd.
- [33] Nathan Schneider, Dirk Hovy, Anders Johannsen, and Marine Carpuat. Semeval-2016 task 10: Detecting minimal semantic units and their meanings (dimsum). In Steven Bethard, Daniel M. Cer, Marine Carpuat, David Jurgens, Preslav Nakov, and Torsten Zesch, editors, *Proceedings of the 10th International Workshop on Semantic Evaluation, SemEval@NAACL-HLT 2016, San Diego, CA, USA, June 16-17, 2016*, pages 546–559. The Association for Computer Linguistics, 2016.
- [34] Xuan Zhang, Pamela Shapiro, Gaurav Kumar, Paul McNamee, Marine Carpuat, and Kevin Duh. Curriculum Learning for Domain Adaptation in Neural Machine Translation. In *Proceedings of the 2019 Conference of the North American Chapter of the Association for Computational Linguistics: Human Language Technologies, Volume 1 (Long and Short Papers)*, pages 1903–1915, Minneapolis, Minnesota, June 2019. Association for Computational Linguistics.
- [35] Friedemann Zenke, Ben Poole, and Surya Ganguli. Continual learning through synaptic intelligence. In Doina Precup and Yee Whye Teh, editors, *Proceedings of the 34th International Conference on Machine Learning*, volume 70 of *Proceedings of Machine Learning Research*, pages 3987–3995, International Convention Centre, Sydney, Australia, 06–11 Aug 2017. PMLR.
- [36] Silvio Franz and Giorgio Parisi. Phase diagram of coupled glassy systems: A mean-field study. *Physical review letters*, 79(13):2486, 1997.
- [37] Luca Saglietti and Lenka Zdeborová. Solvable model for inheriting the regularization through knowledge distillation. *CoRR*, abs/2012.00194, 2020.
- [38] Alex Krizhevsky. Learning Multiple Layers of Features from Tiny Images. 2009.
- [39] Linda B. Smith and Lauren K. Slone. A Developmental Approach to Machine Learning? *Frontiers in Psychology*, 8, 2017.
- [40] Hadar Karmazyn Raz, Drew H. Abney, David Crandall, Chen Yu, and Linda B. Smith. How do infants start learning object names in a sea of clutter? *Annual Conference of the Cognitive Science Society*, 2019:521–526, July 2019.
- [41] Chen Yu and Linda B. Smith. Embodied attention and word learning by toddlers. *Cognition*, 125(2):244–262, November 2012.
- [42] Elizabeth M. Clerkin, Elizabeth Hart, James M. Rehg, Chen Yu, and Linda B. Smith. Real-world visual statistics and infants’ first-learned object names. *Philosophical Transactions of the Royal Society of London. Series B, Biological Sciences*, 372(1711), January 2017.